Image Cover Sheet

CA011274

CLASSIFICATION	SYSTEM NUMBER
UNCLASSIFIED	515893

TITLE

Near-surface environmental limitations to high-frequency sonar performance: a review

System Number:

Patron Number:

Requester:

Notes:

DSIS Use only:

Deliver to:

This page is left blank

This page is left blank

Copy No. 18

DEFENCE R&D DÉFENSE

NEAR-SURFACE ENVIRONMENTAL LIMITATIONS TO HIGH-FREQUENCY SONAR PERFORMANCE: A REVIEW

Mark V. Trevorrow

Defence R&D Canada

Technical Memorandum
DREA TM 2001-002
January 2001

National Defence / Défense nationale

Canada

REPRODUCTION QUALITY NOTICE

This document is the best quality available. The copy furnished to DRDCIM contained pages that may have the following quality problems:

: Pages smaller or Larger than normal

: Pages with background colour or light coloured printing

: Pages with small type or poor printing; and or

: Pages with continuous tone material or colour photographs

Due to various output media available these conditions may or may not cause poor legibility in the hardcopy output you receive.

☒ If this block is checked, the copy furnished to DRDCIM contained pages with colour printing, that when reproduced in Black and White, may change detail of the original copy.

Near-Surface Environmental Limitations to High-Frequency Sonar Performance: A Review

Mark V. Trevorrow
DREA

Defence Research Establishment Atlantic

Technical Memorandum

DREA TM 2001-002

January 2001

Author

Mark V. Trevorrow

Approved by

Ron Kuwahara

Head, Electromagnetics Section

Approved for release by

Walter E. Ellis

Chair, DREA Document Review Panel

Abstract

(U) This work reviews relevant environmental constraints on the performance of high-frequency forward-looking obstacle or mine avoidance sonars. These high-resolution, narrow-beam systems typically operate at frequencies 100 - 500 kHz, focused on detection and classification of near-surface targets up to 500 m range. Relative signal-to-reverberation performance vs. range for a –15 dB surface target is modeled using a generic sonar model approach. Reverberation from and absorption by near-surface micro-bubble layers is shown to create very strong interference. Breaking-wave induced bubbles typically begin to appear above 6 - 10 knots wind speed, with typical bubble density spectra strongly decreasing from 10 to 400 μm radius. At high-frequencies these micro-bubble layers exhibit strong volumetric backscatter, with maximum volumetric back-scattering strengths near –10 dB (re 1 m^{-1}), and maximum extinction losses of order 1 to 10 $dB \cdot m^{-1}$. Detectability of surface targets is limited to less than 20 m at 100 kHz, but the detection range increases with frequency to roughly 250 m at 400 kHz and above. Another significant performance limitation is acoustic refraction by near-surface sound speed gradients commonly found in coastal regions, especially near river-mouths and estuaries and during summer months. The most serious problems arise under downward-refracting conditions with the creation of near-surface acoustic shadow zones. Ray-tracing predictions under typical summer-time coastal conditions show surface shadow regions (i.e. zero detectability) beyond 80 m range. Reverberation from dense zooplankton layers and schooling fish is shown to create minor levels of interference. Reverberation from surface wave roughness scattering in the absence of bubbles is shown to have negligible impact.

Résumé

NC) L'étude examine les contraintes environnementales qui influencent la performance de sonars haute fréquence d'évitement de mines ou d'obstacles. Ces systèmes haute résolution à faisceau étroit sont utilisés habituellement à des fréquences de 100 à 500 kHz pour la détection et la classification de cibles près de la surface à une distance maximale de 500 m. La performance relative signal-réverbération par rapport à la distance pour une cible de surface de -15 dB est modélisée suivant une approche fondée sur un modèle générique de sonar. L'étude montre que la réverbération provenant des couches de micro-bulles près de la surface, et l'absorption par ces couches, produisent un brouillage très marqué. Les micro-bulles produites par le déferlement des vagues commencent habituellement à apparaître lorsque le vent atteint une vitesse de 6 à 10 nœuds, les spectres de densité typiques de bulles diminuant fortement lorsque le rayon des bulles passe de 10 à 400 μm. En haute fréquence, ces couches de micro-bulles présentent une forte rétrodiffusion volumétrique, dont l'intensité maximale avoisine les -10 dB (relativement à 1 m^{-1}), avec des affaiblissements par extinction maximaux de l'ordre de 1 à 10 $dB \cdot m^{-1}$. La détectabilité des cibles de surface est limitée à moins de 20 m à 100 kHz, mais la distance de détection s'accroît avec la fréquence pour atteindre environ 250 m à partir de 400 kHz. Une autre limite de performance importante est la réfraction acoustique par les gradients de vitesse du son près de la surface qu'on retrouve communément dans les régions côtières, en particulier près de l'embouchure des cours d'eau

et des estuaires, et pendant les mois d'été. Les problèmes les plus graves se présentent dans des conditions de réfraction vers le bas, lorsqu'il y a formation de zones d'ombre acoustique près de la surface. Des prédictions par lancer de rayon dans les conditions côtières estivales typiques montrent des régions d'ombre en surface (détectabilité nulle) au-delà d'une distance de 80 m. L'étude montre que la réverbération provenant de couches denses de zooplancton et de bancs de poissons produit de faibles niveaux de brouillage. Elle montre aussi que la réverbération provenant de la diffusion associée à la rugosité des vagues de surface en l'absence de bulles a un impact négligeable.

Executive summary

Introduction
Systems to detect floating mines and avoid near-surface obstacles such as ships, whales, or debris, are important in the development of remote mine-hunting vehicles. Several high-frequency (HF, >100 kHz) multi-beam sonar systems have been proposed for this purpose, yet the performance and limitations of these sonars under typical oceanic conditions is not fully understood. This work reviews recent results from the open literature on HF acoustic scattering from near-surface environmental features such as white-capping, sound speed gradients, and biologics. Performance modeling of a generic sonar system under these conditions is pursued.

Principal Results
Sonar performance vs. range for a −15 dB surface target is modeled. Reverberation from and absorption by near-surface micro-bubble layers due to breaking surface waves is shown to create very strong interference, limiting the detectability of surface targets to less than 20 m at 100 kHz but increasing with frequency to roughly 250 m at 400 kHz and above. Near-surface sound speed gradients commonly found in coastal regions, especially near river-mouths and estuaries, pose serious limitations at all frequencies, with the most serious problems arising under downward-refracting conditions. Ray-tracing predictions under typical summer-time coastal conditions show surface shadow regions (i.e. zero detectability) beyond 80 m range. Reverberation from dense zooplankton layers and schooling fish has the potential to create minor levels of interference.

Significance of the Results
These results predict that sonars operating in the 200 to 400 kHz frequency range are likely to give superior performance against surface targets in the presence of white-capping and biologics, narrowing the choice of obstacle or mine avoidance systems. Furthermore, this study reinforces the need to consider and measure both oceanographic and meteorological conditions during operations requiring obstacle avoidance sonars.

Future Plans
The performance predictions in this work should be verified with field trials performed under a variety of oceanographic and meteorological conditions.

Trevorrow, Mark V. 2001. Near-surface environmental limitations to high-frequency sonar performance: a review. TM 2001-002. DREA.

Sommaire

Introduction
Des systèmes permettant de détecter des mines flottantes et d'éviter des obstacles près de la surface tels que navires, baleines ou débris, sont importants pour le développement de véhicules de déminage à distance. Plusieurs systèmes sonar haute fréquence (HF, >100 kHz) multifaisceaux ont été proposés à cette fin. Toutefois, on ne comprend pas entièrement la performance et les limites de ces sonars dans des conditions océaniques typiques. L'étude examine les résultats récents décrits dans la documentation non classifiée sur la diffusion acoustique HF causée par des éléments environnementaux se trouvant près de la surface tels que les crêtes d'écume des vagues, les gradients de vitesse du son et les organismes biologiques. On cherche à modéliser la performance d'un système sonar générique dans ces conditions.

Principaux resultants
La performance de sonars par rapport à la distance pour une cible de surface de 15 dB est modélisée. L'étude montre que la réverbération provenant des couches de micro-bulles près de la surface et l'absorption par ces couches en raison du déferlement des vagues de surface produit un brouillage très marqué, ce qui limite à moins de 20 m la détectabilité des cibles de surface à 100 kHz, mais la distance de détection s'accroît avec la fréquence pour atteindre environ 250 m à partir de 400 kHz. Les gradients de vitesse du son près de la surface, qu'on retrouve communément dans les régions côtières, en particulier près de l'embouchure des cours d'eau et des estuaires, posent des limites importantes à toutes les fréquences, les problèmes les plus graves se présentant dans des conditions de réfraction vers le bas. Des prédictions par lancer de rayon dans des conditions côtières estivales typiques montrent des régions d'ombre en surface (détectabilité nulle) au-delà d'une distance de 80 m. L'étude montre que la réverbération provenant de couches denses de zooplancton et de bancs de poissons produit de faibles niveaux de brouillage.

Portée des resultants
Ces résultats prédisent que les sonars fonctionnant dans la plage de fréquences de 200 à 400 kHz auront probablement une performance supérieure pour des cibles de surface en présence de crêtes d'écume et d'organismes biologiques, ce qui réduit le choix de systèmes d'évitement d'obstacles ou de mines. En outre, l'étude met l'accent sur la nécessité d'examiner et de mesurer les conditions océanographiques et météorologiques lors d'opérations exigeant des sonars d'évitement d'obstacles.

Suivi
À des fins de vérification, les prédictions de performance fournies par l'étude devraient faire l'objet d'essais pratiques dans diverses conditions océanographiques et météorologiques.

Trevorrow, Mark V. 2001. Near-surface environmental limitations to high-frequency sonar performance: a review. TM 2001-002 DREA.

Table of contents

Abstract i

Résumé i

Executive summary iii

Sommaire iv

Table of contents v

1. Introduction: 1

2. Backscatter from Micro-Bubble Layers: 4

3. Near Surface Refraction: 11

4. Backscatter from a Rough Sea Surface: 15

5. Biological Scattering: 18

6. Summary Discussions: 24

7. References: 26

1. Introduction:

High-frequency (HF, >100 kHz) sonar systems are of developing interest for new Remote Mine-Hunting Vehicles (RMV), Autonomous Underwater Vehicles (AUV), and conventional surface ships. For example, Mine Avoidance Sonars (MAS) are under study for deployment on naval ships, and Obstacle Avoidance Sonars (OAS) have recently been proposed for commercial vessels to avoid collisions with whales. Clearly, AUVs and RMVs require the development of some form of OAS. These HF sonars typically employ 2 or 3 dimensional multi-beam arrays to detect surface and seabed objects in the path of the vehicle. These systems are designed to operate with resolution of order 1 cm in range and 1° in horizontal angle at ranges up to 500 m. HF acoustic systems are largely unaffected by water turbidity providing a great advantage over optical approaches. However, environmental features near the ocean surface impose strong limits on the effectiveness of these near-horizontal looking sonars, especially for the detection of surface targets. The most serious problems arise from acoustic reverberation and extinction due to near-surface air bubbles, and from acoustic refraction due to strong sound speed gradients. These are the focus of this report, along with investigations of ocean surface roughness scattering and biological (fish and zooplankton) interference.

It is generally desirable for an OAS system (this term will henceforth include Mines as an obstacle) to operate at longer ranges, providing greater response times for the vehicle operators. To be useful, a 100 m detection range should be considered a minimum. Many targets of interest can be found on or very close to the sea surface, leading to uncertain detection in the presence of surface reverberation. It is thus desirable to review and investigate sources of this boundary clutter under typical oceanic conditions so that the feasibility of and limitations to target detection can be better understood. The ocean surface is particularly difficult as there are various time-variable factors, such as surface winds, wind-waves, rainfall, ice, tides, freshwater outflow from rivers, and presence of vessel traffic that need to be considered.

The modeling approach pursued here makes only generic assumptions about the type of HF sonar system being utilized and uses relatively simple models of the environmental parameters. Due to the constraints of keeping the transducer arrays to small physical size, only operating frequencies above 100 kHz will be considered. Due to increasing levels of seawater absorption at higher frequencies, 500 kHz is taken as the maximum operating frequency. The modeling will be cast in the general framework of the sonar equation, i.e. for a general backscatter sonar with no time-variable gain, the variation of received echo (intensity) level, *RL*, vs. range, *r*, can be expressed in deciBels (e.g. following Medwin & Clay 1998) as

$$RL = SL + TS - 40\log(r) - 2\alpha \cdot r + BDL(\theta) + TL_{bub} \ , \qquad (1)$$

where *SL* is the transmitter source level, *TS* is the effective back-scatter target strength of the target or scattering mechanism under consideration, α is the seawater absorption at the transmit frequency (calculated using formula due to Francois & Garrison 1982), *BDL* is the beam deviation loss calculated from the transducer transmit and receive beam pattern, and TL_{bub} is the transmission loss due to air bubbles (if present). The HF sonar system is assumed to have a 1° horizontal by 20° vertical beam-pattern oriented with zero elevation angle, looking forward from a vehicle at a mean depth of 3 to 6 m. In either the vertical or

horizontal planes, the two-way beam deviation loss vs. angle can be given by the well-known relation for a line-array

$$BDL(\theta) = 10\log_{10}[D(\theta)], \quad where \quad D(\theta) = \left[\frac{\sin\left(\frac{1}{2}kL_T\sin(\theta)\right)}{\frac{1}{2}kL_T\sin(\theta)}\right]^4, \qquad (2)$$

where k is the acoustic wavenumber, L_T is the transducer dimension (adjusted to maintain a 1° or 20° beam angle at the operating frequency), and θ is the angular deviation from the transducer main axis. The transmit source level is taken as 210 dB (re 1 μPa at 1 m) with a pulse length $\tau = 500$ μs (both are typical values for existing OAS). Water sound speed and absorption values are calculated for typical Canadian coastal conditions with temperature of 10°C, salinity of 32 psu, and sound speed near 1490 $m \cdot s^{-1}$.

An OAS is required to detect at range a wide variety of floating objects, both to avoid damage to the ship or vehicle, and to avoid causing property damage or injuries. Some of the likely targets are:

- Ships: military or civilian vessels of all sizes, both anchored and moving, towed barges (with tow-cable in between)
- Boats: wooden, fiberglass, metal; canoes, kayaks, sailboats
- Fish nets: trawls, seines, gillnets, driftnets, possibly anchored or abandoned
- Floating sea mines, navigation markers, large mooring buoys
- Marine mammals: whales, dolphin, seals, also dead animals
- Seaweed: sea grass or kelp, sometimes concentrated in large rafts
- Driftwood: various sizes up to 1 m diameter x 20 m long

Of the items on this list, the latter two are likely to have to smallest effective target strength and thus be the most difficult to detect. Detection of large ships, particularly those underway and producing wakes, should be straightforward. Also, the detection and avoidance of surface shipping and fishing vessel activity could be assisted by radar, either from the RMV or support ship. The locations of navigation markers and mooring buoys could be programmed into a navigational database. Unattended or abandoned fish nets pose a serious problem for detection, although entanglement in nets would likely not cause significant damage to the ship or vehicle, but would generate considerable down-time. The consequences of a collision with a either a live or dead whale are serious in some cases, both for the ship/vehicle and the whale. Small boats, canoes, and kayaks would likely yield similar target strengths to drifting wood of the same size. Thus, for performance modeling purposes, simple acoustic scattering models can be used to produce approximate estimates of the target strength for all these floating objects. In future these *TS* estimates should be confirmed or refined with field measurements.

Winds and tides can often concentrate floating seaweed and other debris into large shoals or rafts, sometimes as large as 10 to 20 m in size. Sea-grass stems and other small debris pose little threat to ships or vehicles, but large rafts of kelp could potentially impair a RMV/AUV performance or even entrap it. For HF acoustic scattering purposes, a single stem of kelp consists of an air-filled ball roughly 6 cm inside diameter connected to an air-filled cylinder roughly 4 cm diameter by 80 cm length. Some scattering from the leaves or solid parts of

stems (up to 20 m long) will also occur. Air filled objects of this size are nearly perfect acoustic reflectors at high frequencies, and thus the *total* scattering cross-section will equal the geometric area. For an air-filled kelp stem with dimensions as above, the total cross-sectional area is 0.035 m^2 at broadside incidence. The backscatter target strength, *TS*, is then related to the total cross-section by $TS = 10\log_{10}[\sigma_{total}/4\pi]$. Thus the *TS* for a single kelp stem is roughly –26 dB re 1 m^2. A kelp raft large enough to cause problems might be composed of 10 or more stems, so an effective *TS* of –16 dB re 1 m^2 is a reasonable estimate.

In Canadian coastal waters, particularly in the Pacific, floating log-like objects (FLO) are common and present a serious threat to smaller ships and AUV/RMVs. These FLO are roughly cylindrical in shape, and commonly float horizontally although vertical orientation does occur (known as *deadheads*). The smallest FLO which might pose a significant threat to a vehicle will be roughly 0.25 m diameter by 3 m in length. For high frequency acoustic scattering, waterlogged wood should be considered as a penetrable, lossy, elastic material with density and sound speed roughly 800 $kg \cdot m^{-3}$ and 3000 $m \cdot s^{-1}$, respectively. Modeling the FLO as an elastic cylinder, acoustic back-scattering solutions are well-known (e.g. Stanton 1989), and for broadside incidence this 0.25 m diameter by 3 m long FLO will have a back-scatter cross-section of 0.124 m^2 (*TS* = -9 dB re 1 m^2). Now, approximately 20% of the FLO will be above water, so this cross-section should be reduced to 0.099 m^2 (*TS* = -10 dB). The theoretical expression for a lossless, smooth cylinder predicts a highly directional scattering function centered at broadside incidence, however the effect of the rough surface (tree bark) and internal absorption would be to smear the directional response, such that the *TS* at end-incidence might be only 10 dB less. Thus, an average *TS* of –15 dB seems a reasonable estimate for a FLO of unknown (random) orientation relative to the sonar.

2. Backscatter from Micro-Bubble Layers:

At frequencies greater than approximately 5 kHz, acoustic scattering from microscopic air bubbles created by breaking surface waves or ship wakes becomes significant (e.g. Novarini & Bruno 1982; McDaniel & Gorman 1982; Trevorrow et al. 1994). These near-surface bubble layers have been the subject of considerable research over the past 20 years, motivated both by naval interests in understanding surface reverberation and for climatological reasons arising from the fact that these bubbles mediate air-sea gas exchange. Breaking-wave induced bubbles typically begin to appear above 6 - 10 knots wind speed (Thorpe 1982; Crawford & Farmer 1987; Dahl et al. 1997), which is certainly within the typical operating envelope of ships and AUV/RMVs. There is some experimental evidence to suggest that above this 6 to 10 knot threshold near-surface bubble densities increase proportional to the wind-speed cubed (Crawford & Farmer 1987; Wu 1988). Total bubble densities can easily exceed 10^7 per m^3, yet because of their small sizes they typically create total void fractions much less than 0.01%.

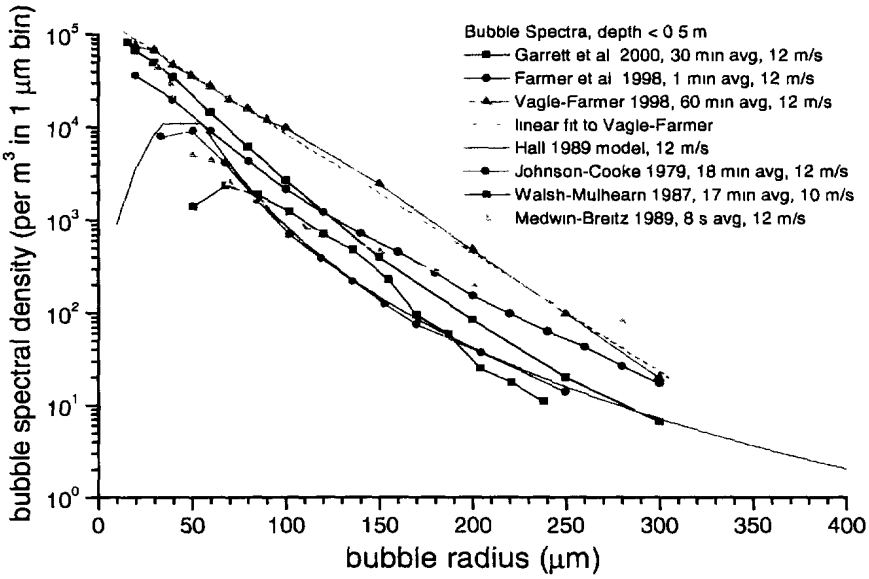

Figure 1: Comparison of measured oceanic bubble size spectra for wind speeds near 12 $m \cdot s^{-1}$, selected or extrapolated to depths < 0.5 m. Averaging times as noted. Johnson & Cooke and Walsh & Mulhearn used photographic techniques. The others are based on acoustic resonator devices. Hall's model is based on Johnson & Cooke data.

These micro-bubble clouds or layers have size vs. density functions, $n(a)$ where a is radius, broadly distributed over the radius interval 10 to 400 μm. Figure 1 shows a comparison of various bubble spectra measurements in the open ocean at wind speeds of 24 knots. The measured bubble size distributions decrease rapidly from peaks near 20 to 50 μm radius (Johnson & Cooke 1979; Walsh & Mulhearn 1987; Medwin & Breitz 1989; Vagle & Farmer 1992, 1998; Farmer et al. 1998), although the exact form of the size-spectra is highly variable and dependent on bubble dissolution, buoyancy, turbulence, fractionation, coalescence and other processes (Thorpe 1982; Garrett et al. 2000). In general, bubbles smaller than 10 μm

radius dissolve and bubbles larger than 200 μm radius have sufficient buoyancy to rise to the surface quickly. Thus, the temporal evolution of a micro-bubble population must be considered, spanning the short bursts of bubble injections by breaking waves to long-time averages of the equilibrium size-spectra. Early work with photographic and acoustic techniques (reviewed by Wu 1988) proposed a power-law dependence on bubble radius, with time-averaged exponents of –4.4. Hall (1989) built a medium-frequency sonar performance model around this power-law dependence (thus accounting for the close agreement in Fig. 1 between Hall's model and Johnson & Cooke data). However, more recent studies have shown a variety of different bubble spectral shapes under different environmental conditions. For example, Medwin & Breitz (1989) found a power-law exponent of –2.7 for larger bubbles (a > 100 μm) directly under (<25 cm below) breaking waves, suggestive that the breaking wave *source spectrum* contains a greater proportion of large bubbles than longer-time averages reported by others. However these source spectra are transient in nature and localized spatially, and for acoustic modeling purposes it is better to use measurements of near-equilibrium size-spectra. Recent measurements with broad-band (5 to 200 kHz) acoustic resonator devices (Vagle & Farmer 1998; Farmer et al. 1998) show size-spectral dependencies closer to exponential variations. For example in Fig. 1 a linear regression (in log-density vs. linear radius) to the Vagle-Farmer data from the open Pacific is well-fit (r = -0.998) by the relation

$$n(a) = 1.6x10^5 \cdot \exp[-a/34\mu m] \quad \text{for} \quad a > 20\ \mu\text{m}. \tag{3}$$

The acoustic resonator measurements generally show greater densities of smaller bubbles (a < 50 μm), presumably highlighting measurement limitations in the older photographic techniques. These high densities of smaller bubbles have been confirmed with coincident inverted echo-sounder measurements at 200 and 400 kHz (Vagle & Farmer 1992, 1998; Trevorrow 1996). Since these smaller bubbles are very important to HF sonar performance, and the older power-law models (e.g. Hall, 1989) are clearly limited in accounting for smaller bubbles, we must favour the Vagle-Farmer model for HF sonar performance assessments. Clearly there is a need here for better reporting of field data on bubble spectral shape at these smaller sizes.

Under typical levels of breaking wave activity these bubbles exhibit spatial and temporal variations that can best be described as *clouds* or *plumes*. In general the bubble plume penetration depth increases with wind speed, but is affected by factors such as near-surface stratification, the presence of Langmuir or convective circulations, and wave conditions. In a time-averaged sense these bubbles can be crudely modeled as a horizontally-uniform, near-surface layer with a vertical exponential decrease with depth scale, L, in the range 0.5 to 1.5 m (Thorpe 1982; Crawford & Farmer 1987; Hall 1989; Trevorrow 1996). Combining this with Eq.(3) yields a simplified bubble size and depth model is thus

$$n(a,z) = n_0 \cdot \exp(-a/34\mu m) \cdot \exp(-z/L) \qquad \text{for } a > 20\ \mu\text{m}$$
$$n(a,z) = n_0 \cdot \exp(-z/L) \qquad \text{for } a < 20\ \mu\text{m}, \tag{4}$$

where n_0 is a surface bubble spectral density (1.6 x 10^5 per m^3 per 1 μm bin at 12 $m \cdot s^{-1}$ wind speed), and z is depth (positive down). Based on field measurements, a wind speed cubed variation can be used to adjust n_0 for wind speeds other than 12 $m \cdot s^{-1}$. Vessel wakes were found to have similar bubble size spectra, localized within a crudely rectangular cross-section along the vessel path, and with a larger exponential depth scale (Trevorrow et al. 1994). Vessel wakes are known to persist for periods up to 15 minutes after the ship passage.

Bubbles exhibit resonant scattering in addition to the usual Rayleigh-geometric type scattering behaviour for spheres. If the bubbles are widely and randomly spaced and non-interacting (a single scattering approximation), the scattering and extinction (sum of absorption and out-of-beam scattering) cross-sections of individual bubbles simply add. In this case the *total extinction* and *total scattering* cross section per unit volume, $S_e(f)$ and $M_v(f)$ (units of m^{-1}), can be calculated as integrals over the product of the bubble size spectra with the acoustic scattering cross-section for a single bubble, e.g. following Medwin & Clay (1998):

$$S_e(f,z) = \int_0^\infty \frac{4\pi \cdot a^2 \delta (k_R a)^{-1}}{\left[(f_R/f)^2 - 1\right]^2 + \delta^2} n(a,z) \cdot da \ , \qquad \text{and} \tag{5}$$

$$M_v(f,z) = \int_0^\infty \frac{4\pi a^2}{\left[(f_R/f)^2 - 1\right]^2 + \delta^2} n(a,z) \cdot da \ , \tag{6}$$

where δ is the bubble total damping constant (see Medwin & Clay for evaluation) and k_R is the acoustic wavenumber at the resonant frequency. The relationship between frequency and bubble size at resonance is given by

$$f_R = (2\pi a_R)^{-1} \sqrt{3\gamma P_0 / \rho_w} \ , \tag{7}$$

where P_0 is the static pressure on the bubble, γ is the ratio of specific heats of the enclosed gas ($\approx$1.4 for air), and ρ_w is the density of the surrounding water. For example with a 100 kHz sonar near the surface, the resonant bubble radius is 34 μm. For HF sonars both the resonant and non-resonant (Rayleigh-geometric) scattering regimes make significant contributions, thus the integral limits in equations 5 and 6 are taken as 0 and 500 μm.

Figure 2 shows typical values of $S_e(f)$ and $M_v(f)$ calculated from Eqs.(4-7) for bubble spectral parameters typically found in the ocean at wind speeds near 16 knots. The figure clearly shows that at frequencies above 10 kHz the near-surface scattering and extinction cross-sections are very high, of order 0.1 to 1 m^{-1} (-10 to 0 dB), with peak values in the 20 to 80 kHz region. This bubble scattering is at least an order of magnitude stronger than other natural scattering sources, such the sea-surface, fish, and zooplankton, and will significantly interfere with the detection of larger objects. For acoustic signals traveling through the bubble layer there is a significant excess acoustic extinction given by

$$TL_{bub}(f,\phi) = 2 \cdot \alpha_{bub} \cdot (path\ length), \quad \alpha_{bub} = 4.34 \cdot S_e(f,z) . \tag{8}$$

This bubble loss applies equally to backscatter from the bubble layer, surface roughness scattering, or any targets within the surface bubble layer. The variation of α_{bub} with frequency, compared to the standard seawater absorption term α, is shown in Figure 2. Clearly, between 10 kHz and 100 kHz the excess extinction due to bubbles is very strong, of the order 1 to 10 $dB \cdot m^{-1}$, greatly exceeding the seawater absorption at frequencies up to 300 kHz. Note that these predictions are for moderate winds just above the onset of white-capping, and that at higher wind speeds these bubble effects will be even stronger.

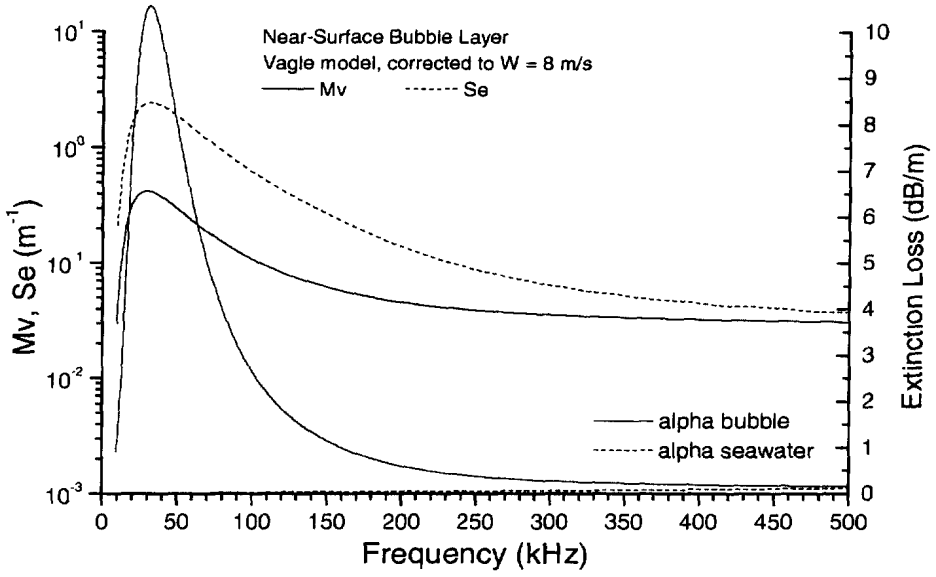

Figure 2: Variations of total scattering and extinction volumetric cross-sections with frequency for bubble model in Eq. 7, with $n_0 = 4.7 \times 10^4$ per m^3 (re 1 μm bin) and $L = 0.5$ m, evaluated at depth $z = 0.2$ m. Also shown in red is the corresponding bubble and seawater extinction loss.

The general expressions for bubble scattering and extinction can be adapted for the case of low-grazing angle back-scatter from a near-surface bubble layer. The backscatter target strength of a vertical slice through the bubble layer (neglecting extinction and beam pattern effects) is given by a depth integral of $M_v(f,z)$ multiplied by the insonified beam horizontal area, i.e.

$$TS_{bub} = 10\log_{10}\left[\tfrac{1}{4\pi}\int_0^\infty M_v(f,z)\cdot dz\right] + 10\log_{10}\left[\tfrac{1}{2}\cdot c\cdot\tau\cdot r\cdot\varphi\right] \text{ (dB)}, \qquad (9)$$

where c is the sound speed, τ is the pulse length, and φ is the transducer horizontal beam-width (to -3dB, in radians). An important characteristic of bubble scattering layers under this geometry is that for small grazing angles (i.e. longer ranges), the path through the bubble layer is relatively long, so that the extinction greatly exceeds the volume scattering terms. This creates a decreasing echo scattering strength (TS_{bub} - TL_{bub}) at greater range, even though the insonified volume increases linearly with range. Thus, the vertical variations of M_v, S_e, and BDL must be included together in the calculation of the total scattering strength from the layer at any given range. This implies, substituting for several terms in Eq.(1), a vertical integral of the form

$$TS + TL_{bub} + BDL(\theta) = 10\log_{10}[\sigma], \quad \text{where}$$

$$\sigma = \tfrac{1}{2}\cdot c\cdot\tau\cdot r\cdot\varphi\cdot(4\pi)^{-1}\int_0^\infty M_v(z)\cdot D(\theta)\cdot\exp\left[-2\cdot S_e(z)\cdot L/\sin(\phi)\right]\cdot dz\,. \qquad (10)$$

In this case ϕ and θ are evaluated as a function of depth given the sonar geometry. In this integral, bubble back-scatter contributions will be much larger near the surface, but this is balanced by much stronger extinction as the surface is approached. In this model, surface-reflected multi-paths are ignored because they will suffer surface reflection losses and extra bubble extinction.

An alternate formulation is based on a semi-empirical approach, as advocated by a report from the Applied Physics Laboratory at the University of Washington, Seattle (APL-UW 9407), and earlier models proposed by McDaniel & Gorman (1982) and McDaniel (1993). These models use an incoherent summation of direct and surface-reflected multi-paths along with a resonant bubble approximation (ignores geometric scattering contribution), including both scattering and extinction effects. For this APL-UW 9407 model the target strength and bubble transition loss terms become:

$$TS + TL_{bub} = 10\log_{10}\left[\frac{\beta_v}{4\pi}\frac{\delta_r}{\delta}\left(\frac{1+8\beta\exp(-2\beta)-\exp(-4\beta)}{2\beta}\right)\right] \qquad (11)$$

where $\beta = \beta_v/\sin\phi$, δ_r is the bubble damping constant at resonance (= 0.0136), and the quantity β_v is related to the depth-integrated density of resonant-sized bubbles. This parameter has been estimated from a large set of surface scattering data as a function of frequency (f, kHz) and wind-speed (U, m·s^{-1}), with result

$$\beta_v = \begin{cases} 10^{-5.2577+0.4701U}(f/25)^{0.85} & for \quad U < 11\,m/s \\ \beta_v(U=11)\cdot(U/11)^{3.5} & for \quad U \geq 11\,m/s \end{cases} . \qquad (12)$$

Note that this model predicts a low level of bubble scattering at very low wind speeds, counter to our *a priori* expectation of a bubble production threshold near 3 to 5 m·s^{-1}. On the basis of comparisons with field data this APL-UW model is considered accurate between 10 and 80 kHz, which is also the range of validity for the resonant bubble approximation.

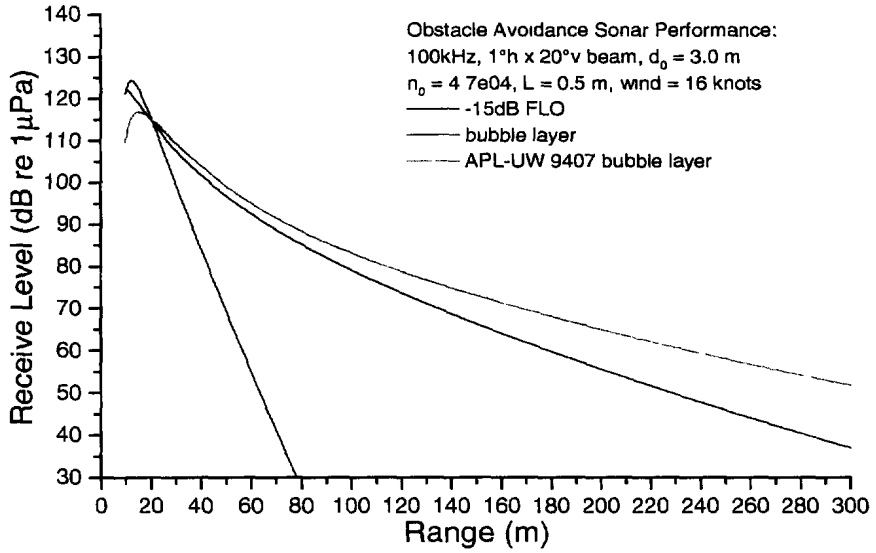

Figure 3: Comparison of receive level vs. range predictions for 0.25 m dia. x 3 m long FLO with bubble layer scattering for a 100 kHz sonar at 3 m depth. Bubble layer parameters as in Fig. 2.

Figures 3 and 4 show the receive levels predicted for scattering at 100 and 400 kHz from a FLO as compared to these two models for bubble layer scattering. As discussed above the FLO has an expected *TS* near –15 dB, assuming that the entire object is within the sonar beam. At both frequencies the two models for bubble layer scattering are in approximate agreement. In the 100 kHz case (Fig. 3) the APL-UW model shows higher scattering strength

at longer ranges, presumably due to the inclusion of surface-reflected multi-paths. Conversely at 400 kHz (Fig. 4) the APL-UW model gives a lower prediction due to the neglect of off-resonant bubble scattering. The combination of acoustic extinction reducing the echo from the FLO and the strong backscattering from the bubble layer itself strongly interferes with the detectability of the FLO. For a 100 kHz system (Fig. 3) there is only a small range interval (<20 m) where the FLO would be detectable above the bubble layer scattering, rendering it essentially useless for OAS operations. At higher frequencies (e.g. at 400 kHz in Fig. 4), the maximum detection range extends to as much as 240 m owing to the lower levels of bubble extinction. However, both the FLO and bubble layer receive levels at longer ranges are lower for the 400 kHz case due to the increased seawater absorption.

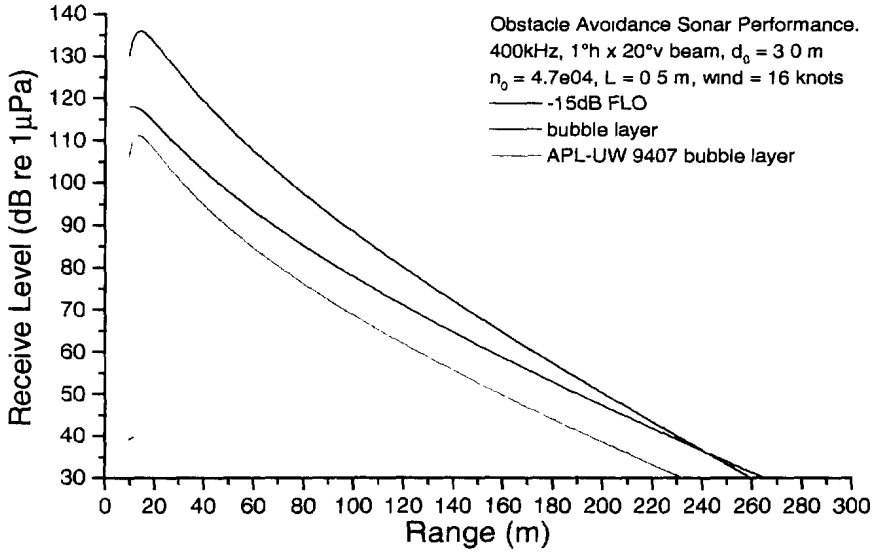

Figure 4: Comparison of receive level vs. range predictions for 0.25 m dia. x 3 m long FLO with bubble layer scattering for a 400 kHz sonar at 3 m depth. Bubble layer parameters as in Fig. 2.

A useful parameter to summarize the detectability of floating objects in the presence of a surface bubble layer is the signal excess, $RL_{FLO} - RL_{bubble}$, as shown in Figure 5 for several possible OAS operating frequencies. A detection threshold of 0 dB is optimistically given, based on the idea that the FLO shape and ping-to-ping persistence would allow detection at relatively low signal-to-reverberation ratios. Clearly, with increasing sonar frequency the detectability at range improves, to the point where detection becomes limited by other factors such as internal systemic noise and dynamic range limitations. As can be seen in Figure 4, even though there is a positive signal excess relative to bubble scatter up to 240 m range, owing to strong bubble extinction the *RL* of the FLO has dropped to nearly 110 dB below its near-range maximum. Receiver signal to noise performance near 110 dB is a realistically achievable upper bound for HF sonar electronics. Thus, at frequencies above 400 kHz the combination of bubble extinction and seawater absorption will limit detection range to less than approximately 240 m.

Clearly these OAS performance predictions are sensitive to the sonar depth, with the effective path lengths through the bubble layer decreasing if the sonar is deployed at greater depth. Generally, the choice of operating depth is determined by the design of the vessel or

vehicle, however it is clear that mounting the sonar deeper yields improved performance. Figure 6 shows the effect on OAS performance by doubling the sonar depth to 6 m. In this situation there is a transducer sidelobe effect at closer range, but otherwise the performance is improved. For example at 200 kHz the effective detection range increases from 100 m to 160 m. Also, for the higher frequencies the overall bubble layer losses are reduced so that the FLO *RL* does not drop to 110 dB below the maximum until ranges in excess of 300 m.

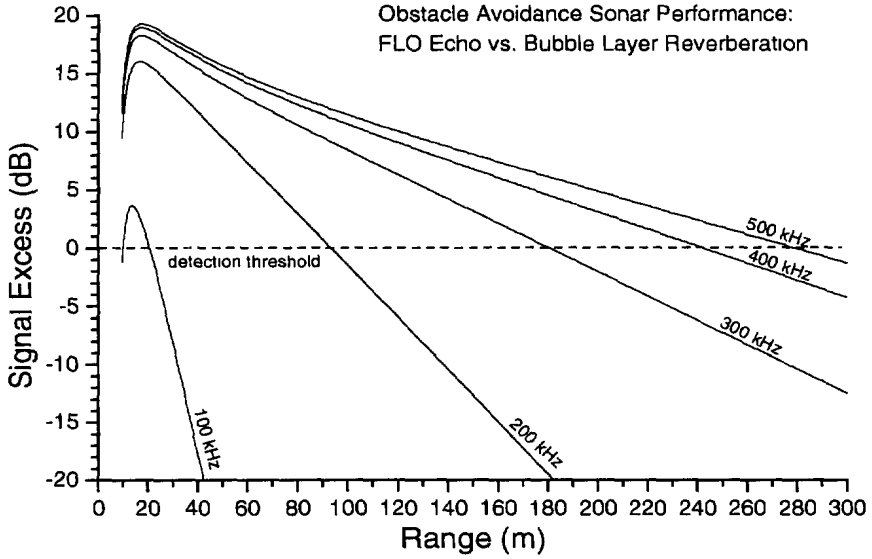

Figure 5: Signal excess vs. range for case of TS = -15 dB FLO in presence of bubble layer for 100 – 500 kHz sonar frequencies, using sonar at 3 m depth and bubble model in Eqs. 4-10.

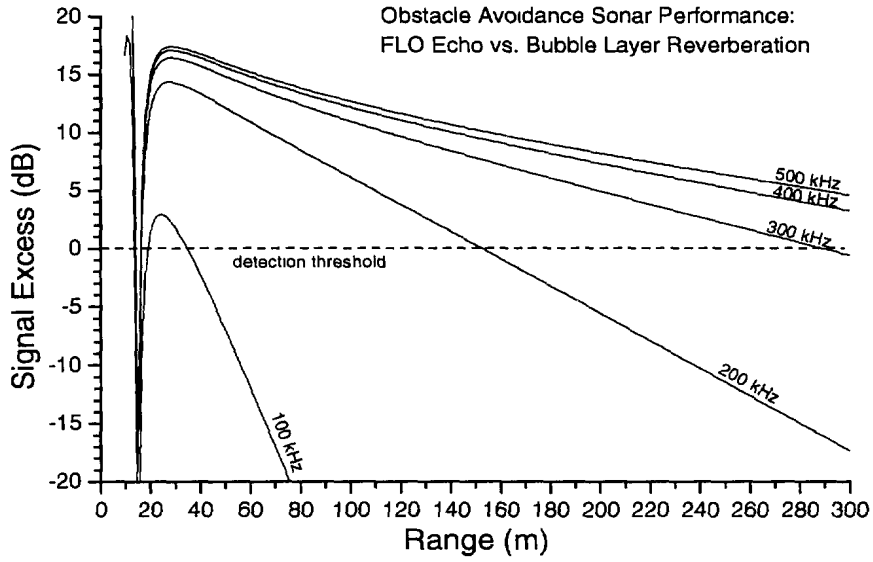

Figure 6: Signal excess vs. range for case of TS = -15 dB FLO in presence of bubble layer for 100 – 500 kHz sonar frequencies, using sonar at 6 m depth and bubble model in Eqs. 4-10.

3. Near Surface Refraction:

A common feature of coastal environments are strong, near-surface gradients in both temperature and salinity, which directly affect sound speed. These sound speed gradients can be both positive and negative, and in both cases will significantly interfere with OAS performance. Under calm conditions (i.e. without wind-wave mixing), riverine outflows or estuarine circulations create strong salinity and temperature stratification. An example of this is shown in Figure 7. In this situation there were strong downward-refracting conditions created by the warm yet fresh Fraser River outflow as it mixed with the ambient waters of the Strait of Georgia (near Vancouver, B.C.). Within the upper 3 m the average sound speed gradient was -1.5 s^{-1}, with a stronger gradient (-3.2 s^{-1}) between 5 and 7 m depth. In this case the effects of increasing temperature (increases sound speed) dominate over the decreasing salinity near the surface. This case of a warmer surface layer will be quite common in the summer in many locations, with generally light winds and strong solar heating. A similar situation can exist in more open coastal waters, as shown for example in Figure 8 with a profile taken from the central Oregon coast in Sept. 1995. Conversely, situations exist (for example in a glacially fed fjord) where a colder, fresher surface layer can generate strongly positive sound speed gradients, creating upward-refracting conditions.

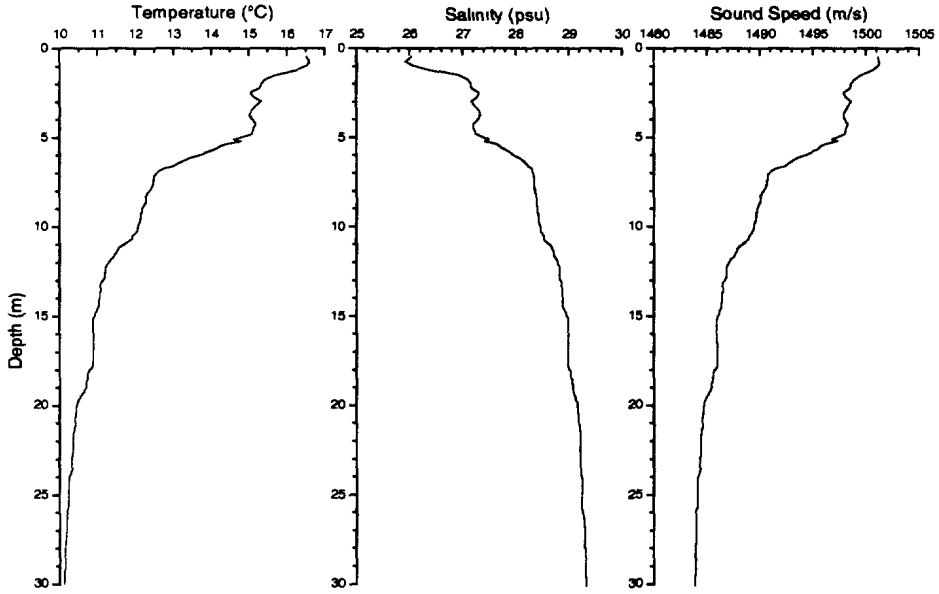

Figure 7: Temperature, salinity, and sound speed profiles taken in south-eastern Strait of Georgia, near mouth of Fraser River, near Vancouver, BC, on Sept. 14, 1999.

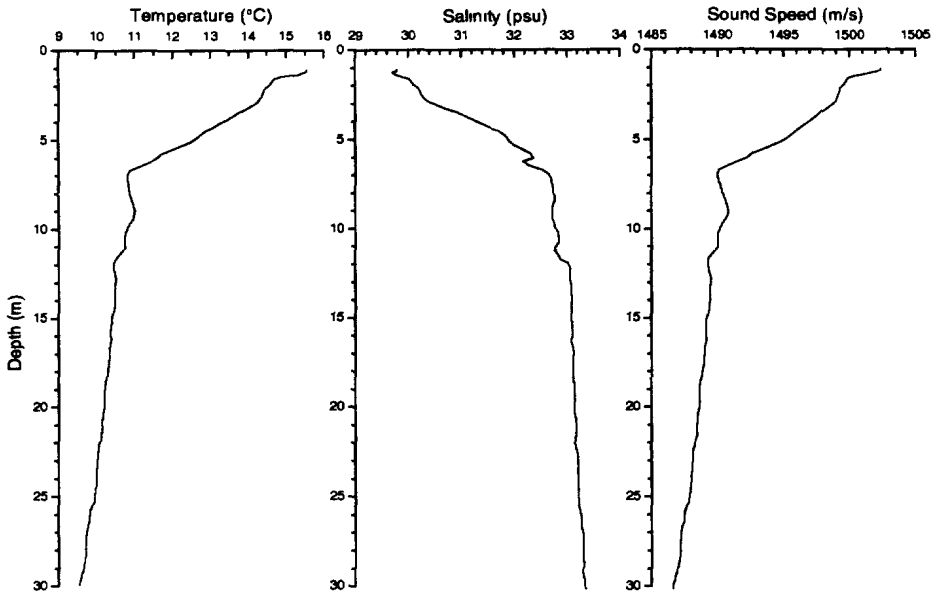

Figure 8: Temperature, salinity, and sound speed profiles taken approx. 10 km off the coast of central Oregon, USA, in Sept. 18, 1995.

An alternate source of sound speed gradients under windy conditions, where wind-wave mixing would likely destroy any near-surface stratification, is the void fraction effect of the resultant bubble layer. Air has a sound speed roughly 5 times less than seawater, thus at low frequencies (<20 kHz) the resultant bulk sound speed of bubbly water is greatly reduced, creating upward-refracting conditions. At frequencies above the dominant bubble resonances (>100 kHz) the sound speed anomaly is positive and asymptotically tends to the bubble-free value. In between these limits the bubble resonances create a complicated behaviour in the bulk sound speed, given by standard models (e.g. Medwin & Clay, 1998) as:

$$c = c_0\left[1 - 2\cdot\pi\cdot c_0^2\int_0^\infty \frac{y^2(y^2-1)}{2\cdot\pi\cdot f_r^2[(y^2-1)^2+\delta^2]}\cdot a\cdot n(a,z)\cdot dz\right], \qquad (13)$$

where c_0 is the sound speed in bubble-free seawater and $y = f_r/f$. In the 10 to 500 kHz region this bulk sound speed becomes dispersive (frequency dependent), with the sound speed anomaly initially negative then switching to positive above approximately 40 kHz. Figure 9 shows the predicted variation of this bulk sound speed with frequency at the sea surface for the same bubble layer densities as examined in Figs. 2-6. At frequencies of interest herein (100 – 500 kHz) the bubble-induced sound speed anomaly is downward-refracting and of similar magnitude to the temperature and salinity effects shown in Figs. 7 and 8. The depth variation of sound speed will show the same exponential decay scales (i.e. L = 0.5 to 1.5 m) as the bubble densities. Under open ocean conditions with slightly higher wind speeds (15 to 20 knots) and actively breaking wave conditions, Lamarre & Melville (1994) measured sound speed anomalies at low frequencies (near 10 kHz) within the upper 0.5 m occasionally exceeding 100 ms^{-1}.

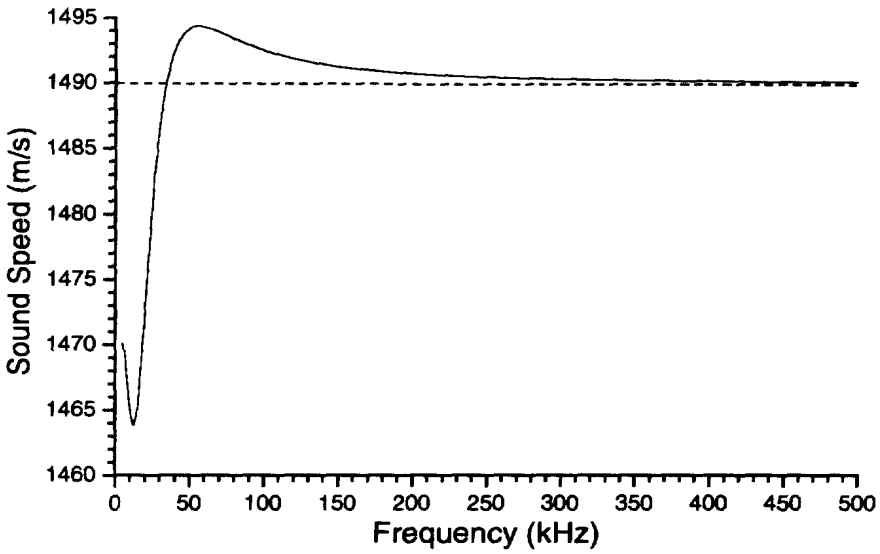

Figure 9: Near-surface sound speed vs. frequency due to bubbles. Uses bubble spectrum model as in Eq.(7) at $z = 0$, with $n_0 = 4.7 \times 10^4$ per m^3 (re 1 μm bin) and $c_0 = 1490$ m·s^{-1}.

Regardless of the source of the sound speed variations, the refraction effects on OAS performance in this near-horizontal geometry will be significant. Note that for the case of temperature-salinity stratification these refraction effects are independent of frequency, whereas for the bubble-layer effect there is dispersion. For HF acoustic propagation ray-tracing methods are appropriate, and can be used qualitatively to identify shadow and convergence zones created by these sound speed profiles. Similar to the bubble layer calculations above, a 20° vertical aperture oriented horizontally from a source depth of 3 m is used. In this model the sea-surface is assumed flat and perfectly reflecting, which is reasonable for calm conditions but will be inaccurate for windy conditions (i.e. the bubble layer case). Both downward and upward-refracting cases are examined. For the downward-refracting case, the sound speed profile in Fig. 7 is used, with resultant ray-tracing diagram shown in Figure 10. In this situation the effects of refraction begin to appear beyond roughly 40 m range. There is an acoustic *shadow* region for near-surface targets beginning at roughly 70 m range, with a strong sub-surface convergence zone between 80 and 200 m. Beyond 200 m range the entire beam is focused downwards to depths greater than 5 m. Clearly this situation is disastrous for detection of near-surface targets. Also, for sub-surface targets beyond approximately 30 m range there will appear a surface-reflected multi-path in addition to the direct path.

The ray-tracing diagram for an equivalent upward-refracting situation, given by a linear profile increasing from 1485 m·s^{-1} to 1490 m·s^{-1} in the upper 5 m and constant thereafter, is shown in Figure 11. Here rays launched upwards or near horizontal (angles ≥ 0) are trapped within a near-surface waveguide, refracted upwards and repeatedly reflected from the sea-surface. In this scenario there are distinct surface convergence and reflection zones recurring roughly 180 m apart. In contrast to the downward-refracting case there are no near-surface shadow regions, however a sub-surface shadow-zone appears near 5 m depth beyond 150 m range. The upwards refraction also increases the effective surface grazing angle at a given

range, enhancing the surface roughness back-scattering which might become more significant in the absence of a bubble layer. Similarly, for sub-surface targets beyond roughly 30 m range there will generally exist a surface-reflected multi-path in addition to the direct path.

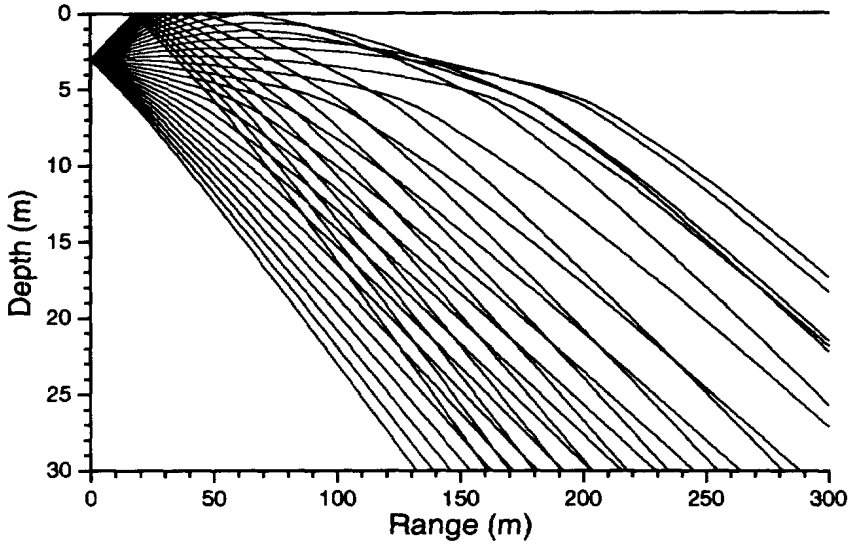

Figure 10: Ray-trajectories vs. range and depth for downward-refracting sound speed conditions as shown in Fig. 5. Ray-trace follows 31 rays launched between ±10° (0.66° spacing).

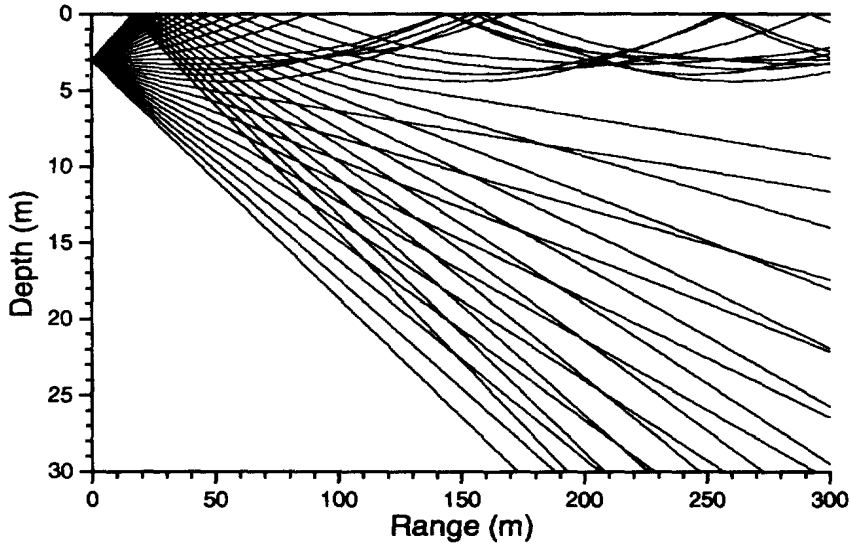

Figure 11: Ray-trajectories vs. range and depth for upward-refracting sound speed conditions. Ray-trace follows 31 rays launched between ±10° (0.66° spacing).

4. Backscatter from a Rough Sea Surface:

For the HF sonar geometry under consideration herein, the narrow acoustic beam intersects the rough sea-surface at small grazing angles, typically much less than 10°. For acoustic backscatter from the sea-surface the *effective* target strength is strongly dependent on grazing angle and interfacial roughness, and increases in proportion to the insonified area projected onto the surface, i.e. as

$$TS_{surface} = SS(\phi) + 10\log_{10}\left[\tfrac{1}{2}\cdot c\cdot\tau\cdot\cos\phi\cdot r\cdot\varphi\right], \qquad \text{(dB)} \qquad (14)$$

where $SS(\phi)$ is the interfacial Scattering Strength (dB) at grazing angle ϕ. Extensive theoretical and experimental investigations of this interfacial scattering strength have been conducted since the 1950's, for both ocean surface and sediment reverberation (see Fortuin 1970 and McDaniel 1993 for literature reviews). Much of this work has been focused on the frequency range 100 Hz to 10 kHz, motivated by long-range naval sonar developments. A fundamental reverberation model, first derived by Lord Rayleigh, assumes Bragg diffraction from a random surface with small-scale roughness (i.e. roughness scales << acoustic wavelength and small surface slopes), with general form (McDaniel 1993)

$$SS(\phi) = 10\log_{10}\left[\tfrac{2}{\pi}\cdot k^4\cdot\sin^4\phi\cdot W(K)\right] \qquad \text{(dB)}, \qquad (15)$$

where k is the acoustic wavenumber and $W(K)$ is the wavenumber spectrum of the surface roughness in the direction of the acoustic beam, with $K = 2k\cos\phi$. At high acoustic frequencies considered herein, the roughness scales causing this reverberation are of order millimeters to centimeters (gravity-capillary waves). Appropriate forms of $W(K)$ in this very high wavenumber regime are still a subject of some debate. For medium frequencies (1 to 60 kHz), the wavenumber spectrum varies approximately as k^{-4}, making the surface scattering strength independent of frequency, in accordance with measurements.

In general, sea-surface roughness will exhibit a broad range of scales, with the longer scales having much larger amplitude. To handle this a composite-roughness model has been proposed such that the surface can be partitioned into two (large and small scale) wavenumber regimes. The longer waves then modulate the back-scattering from the acoustically important shorter waves through two mechanisms: (i) by *tilting* the surface thus modifying the grazing angle (note that Eq.15 is very sensitive to ϕ), and (ii) by *shadowing* some portions of the surface at low grazing angles. This modeling approach has been successful in radar applications. Modified for these two mechanisms, the Rayleigh composite-roughness model has the form (e.g. McDaniel & Gorman, 1982)

$$SS(\phi) = 10\log_{10}\left[\tfrac{2}{\pi}\cdot S(\phi)\cdot k^4\cdot\sin^4\left(f(\phi)\right)\cdot W(K)\right] \qquad \text{(dB)}, \qquad (16)$$

where $S(\phi)$ accounts for surface shadowing [$0 < S(\phi) < 1$] and $f(\phi)$ is an *effective* grazing angle adjusted for tilting of the larger scale surface [$f(\phi) > \phi$] (see McDaniel & Gorman 1982 and McDaniel 1993 for evaluation of these parameters). The combination of these expressions leads to backscatter predictions that increase strongly with wind speed and slowly with acoustic frequency. One should note that typical coastal environments will be *fetch limited*, such that the large-scale wave heights will be reduced but the wave steepness and wind stress will be greater than in a fully developed sea.

The APL-UW 9407 report also prescribes a semi-empirical formulation for surface roughness scattering. In this model the surface scattering can be divided into two regimes, one due to Rayleigh-type scattering at low grazing angles and the other due to reflections

from wave facets at angles nearer to normal incidence ($\phi > 70°$). The roughness scattering strength is given by the simple formula:

$$SS_r(\phi,U) = 10\log_{10}[\sigma_r], \quad \sigma_r = 1.3x10^{-5} \cdot U^2 \cdot \tan^4\phi . \tag{17}$$

The surface roughness regime is frequency-independent due to the k^{-4} dependence in the surface wavenumber spectrum. The facet scattering component is given by:

$$SS_f(\varphi,U) = 10\log_{10}[\sigma_f], \quad \sigma_f = \frac{\sec^4\psi}{4\pi s^2} \cdot \exp\left[\frac{-\tan^2\psi}{s^2}\right] \tag{18}$$

where $\psi = 90° - \phi$ is the incidence angle and the mean-square surface slope, s^2, is given by

$$s^2 = \begin{cases} 4.6x10^{-3} \cdot \ln[2.1 \cdot U^2] & U > 1\,m/s \\ 0.0034 & U < 1\,m/s \end{cases} . \tag{19}$$

APL-UW 9407 provides a formula for interpolating between these two scattering regimes at intermediate grazing angles. The APL-UW model also specifies that the bubble scattering contributions as outlined in Eqs. 11-12 should be added to the surface scattering terms (Eqs. 17-19), even at low wind speeds, and furthermore that the surface scattering cross-sections must be reduced by a bubble extinction term.

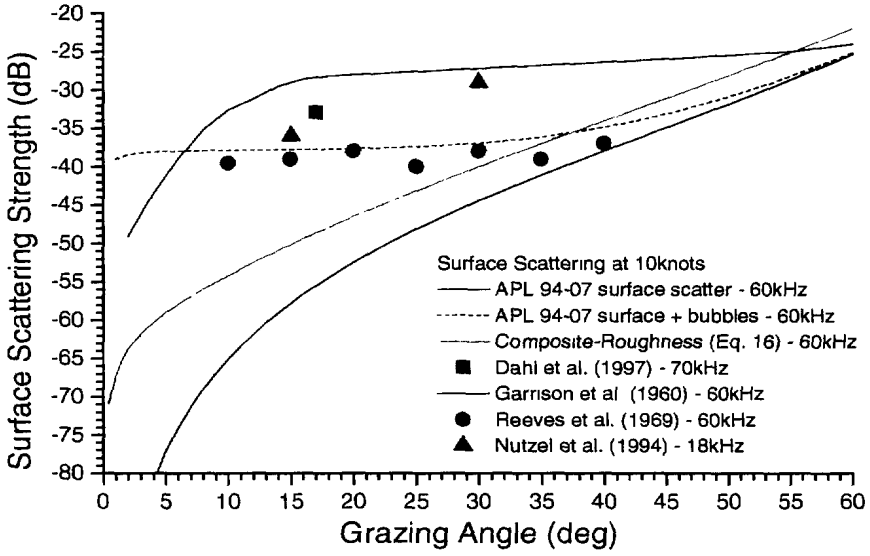

Figure 12: Comparison between surface roughness scattering measurements and models as a function of grazing angle for medium-frequency sonars near 10 knots wind speed.

For the case of low-grazing angle sea-surface backscatter the experimentally measured surface scattering strengths generally exceed the composite-roughness and APL-UW surface scattering predictions over a broad frequency and wind speed range. An example for medium frequency sonars at winds near 10 knots is shown in Figure 12. There are surprisingly only a few measurements of ocean surface backscatter at medium acoustic frequencies and low grazing angles (e.g. Garrison et al. 1960; Reeves et al. 1969; Nutzel et al. 1994; Dahl et al. 1997). A common problem encountered with such measurements is the occurrence of near-surface air bubbles, which is an issue that earlier investigators had not realized. In Fig. 12 the two surface scattering models under-predict the measured values by 15 to 20 dB at low

grazing angles (of interest here), however the APL-UW model with the addition of bubbles is a much better match. Furthermore, Dahl et al. (1997) show through simultaneous comparison of acoustic and radar scattering at the same wavelength from the same area of ocean that a bubble creation threshold exists at winds of 3 to 5 $m \cdot s^{-1}$ (6 to 10 knots). It must be concluded that these earlier measurements of low-grazing angle surface scattering were unknowingly contaminated by bubble scattering. At higher grazing angles (>60°) the total backscatter becomes dominated by the facet scattering component, surpassing even the bubble layer scattering. Finally, the available data are insufficient to specify any frequency dependence or change in these surface scattering regimes at frequencies above 100 kHz.

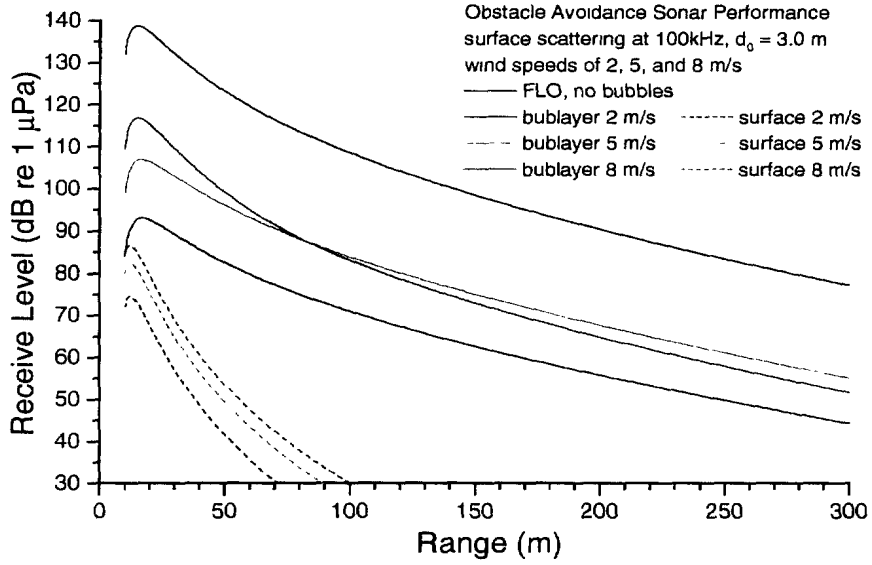

Figure 13: Comparison of receive level vs. range predictions between surface-roughness scattering and bubble layer scattering at several wind speeds with echo from a TS = -15 dB FLO. Roughness and bubble layer models from APL-UW 9407 for a 100 kHz sonar at 3 m depth.

In general, surface roughness scattering is largely inconsequential for detection of large (*TS* = -15 dB) surface targets, as shown in Figure 13. Signal excesses from 28 dB increasing with range to 80 dB at 300 m are predicted for detection of an FLO at a variety of relatively light winds. The surface roughness scattering decreases strongly at greater range due to the strong sensitivity of the models to diminishing grazing angle (e.g. $\tan^4\phi$ in Eq. 17). Also note in the bubble layer scattering predictions for winds of 8 $m \cdot s^{-1}$ there is a decrease in the receive level at greater range, attributable to bubble extinction effects.

5. Biological Scattering:

In general, biological targets will only be significant for HF sonar operation if they occur in large numbers. Large individual fish (such as Pacific salmon) can have *TS* up to –20 dB re 1 m^2, making them readily detectable with OAS systems, however their typical natural abundance is relatively low (< 1 x 10^{-6} per m^3). Fish might congregate in certain areas at certain times of the year, for example with salmon migration at the mouth of the Fraser River near Vancouver, B.C., but in general non-schooling fish will not pose any significant problems. Conversely, near-surface schooling fish (such as herring or sardines) can occur with sufficient numbers and densities to present a strong and spatially large acoustic target. For example Trevorrow and Pedersen (1999) using 100 kHz sidescan sonars measured total target strengths up to –10 dB re 1 m^2 for 26 cm long herring in roughly circular schools up to 20 m diameter. Figure 14 shows an example of a near-surface herring school taken with a 120 kHz echo-sounder. The school is the compact object from 5 to 18 m depth, with duration in the beam of approximately 15 s, corresponding to an along-track dimension of 30 m. Note that the school partially shadows echoes from the deeper zooplankton layers, and exhibits an acoustic decay at the lower edge indicative of acoustic multiple scattering (ringing) within the school. The volumetric scattering strength with the school is in excess of –31 dB re 1 m^{-1}. Since adult herring have individual dorsal-incidence target strengths near –41 dB re 1 m^2, this indicates fish densities within the school in excess of 10 per m^3. Assuming this school is roughly circular in planform, our generic 1° x 20° horizontal sonar would see this school at (for example) 100 m range as a –19 dB target of horizontal dimension 30 m. This would be clearly detectable with a HF sonar except under heavy bubble layer activity.

Zooplankton are another source of interference, sometimes occurring in very high density swarms near the ocean surface, particularly at night. Some of the common zooplankton species found in coastal waters are listed in Table I. It is expected that the scattering layers relevant to HF sonar operation, and particularly those exhibiting diurnal migrations to the near-surface region, will be composed of crustacean zooplankton such as euphausiids (krill), amphipods (brine shrimp), and various other shrimp species. Because of their relatively large size, high abundance, and nocturnal migration to the near-surface region, euphausiids are likely to be the most acoustically significant family. Particularly in the spring and early summer euphausiids can form dense swarms near the ocean surface, with densities up to 5000 per m^3. Euphausiids are joined in their diurnal migrations by amphipods and larger shrimp, however these are generally found deeper or on the bottom during the day and migrate only to the mid-water during nighttime. Commonly the daytime depth-extent of the euphausiids is near 80 to 100 m. Other species of Pteropods, Chaetognaths, Ctenophores, and Cnidaria also diurnally migrate from the surface through depths of 250 m. However in the context of HF sonar operation these can be largely ignored due to their low abundance and small target strength (most are soft- or gelatinous-bodied animals). The exception to this are the hard shelled planktonic Pteropods *Limacina helicina* and *L. retroversa*, which for typical sized animals near 1 mm esr have a *TS* at 200 kHz near –84 dB (Stanton et al. 1994), more similar to that of small euphausiids.

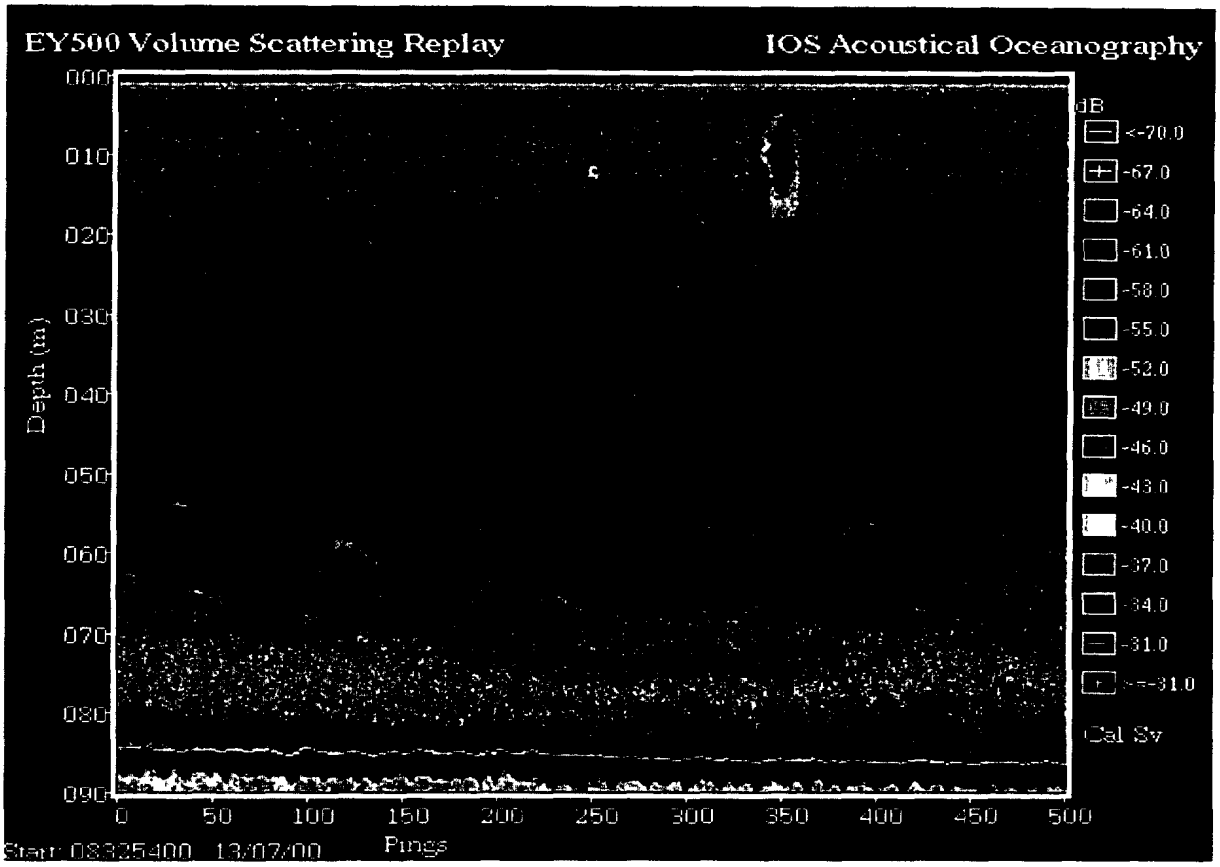

Figure 14: 120 kHz echo-sounder depth vs. time record, showing calibrated volumetric back-scatter strength (dB re 1 m^{-1}). Data collected near the Kenai Peninsula, Alaska, July 13, 2000. Echo-sounder operated at 0.4 s per ping from a vessel traveling at 2 $m \cdot s^{-1}$.

Table I: Expected zooplankton species, sizes, and densities within the upper 100 m of typical coastal waters. Target strengths taken from measurements or empirical relations (see references).

Family	**Typical Size** (mm)	**TS @ 200kHz** (dB re 1 m^2)	**Typical Density** (per m^3)
Euphausiids (krill)	5 to 20	-82 to -72	1 to 5000
Amphipods (brine shrimp)	5 to 15	-82 to -75	0.1 to 20
Shrimp (Decapods, Mysids)	10 to 90	-80 to -53	< 1.0
Copepods	2 to 6	-94 to -88	100 to 10000
Pteropods (snails)	1 to 10	-96 to –84	0.01 to 500
Chaetognaths	10 to 25	-95 to -89	1.0
Siphonophores	10 to 20	-90 to -84	< 1.0
Medusae/Cnidarians (jellyfish)	50 to 100	?	0.5 to 5.0
Appendicularians/Larvaceans	1.0	-110	100 to 10000

The most abundant species in both the coastal and oceanic waters are copepods (families *Calanus*, *Neocalanus*, *Pseudocalanus*, *Euchaeta*, *Metridia*), with adults reaching typical lengths of 4 mm and in some species up to 6 mm. *Neocalanus plumchrus* appears to be the most common species in B.C. coastal and NE Pacific waters. These species generally do not

migrate on a daily basis, but rather they each have a strong seasonal growth and migration cycle. For example, young of *N. plumchrus* feeding on the spring bloom of phytoplankton grow rapidly in size and population in mid- and epi-pelagic zones (surface to 100 m) in the March through June period, then the adults dive to deep waters (>300 m) for the remainder of the year.

An example of very high near-surface zooplankton densities is shown in Figure 15, taken from the highly productive area near the ice-edge in the Chukchi Sea (NW Alaska coast). Obvious in the figure is an intense, cloud-like layer 5 to 20 m deep likely composed of euphausiids (krill). This near-surface zooplankton layer has peak volume scattering strengths near –43 dB re 1 m^{-1}. Assuming this layer to be composed of adult euphausiids (*TS* = -72 dB) yields a maximum abundance near 800 per m^3.

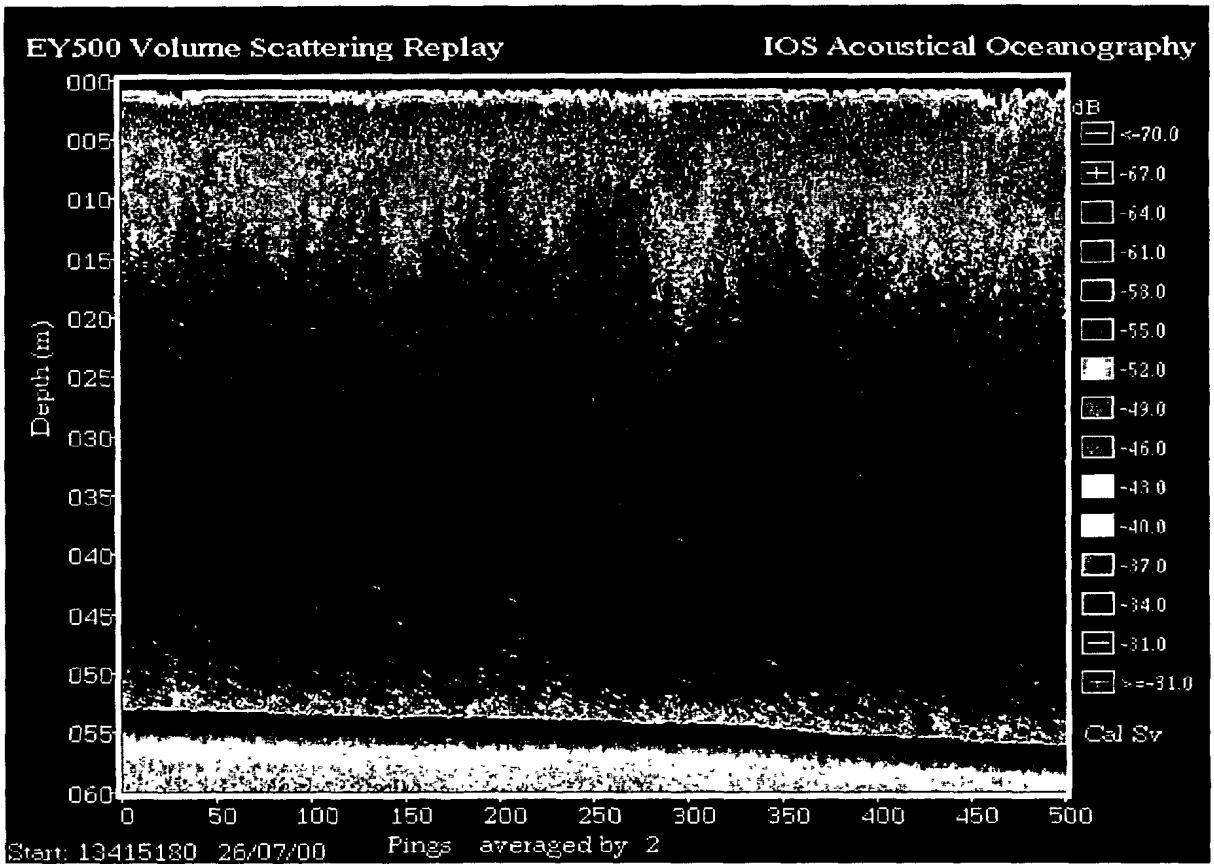

Figure 15: 120 kHz echo-sounder depth vs. time record, showing calibrated volumetric back-scatter strength (dB re 1 m^{-1}). Data collected near in the Chukchi Sea near Pt. Barrow, Alaska, July 26, 2000. Echo-sounder operated at 0.4 s per ping, with 2 ping average, from a vessel traveling at 2 $m \cdot s^{-1}$.

Detailed modeling and measurement of zooplankton scattering is a difficult business, and has been pursued by only a few investigators (see e.g. Johnson 1977; Greenlaw 1977; Holliday & Pieper 1980; Kristensen & Dahlen 1986; Greene et al 1989; Stanton 1989; Wiebe 1990; Macaulay 1994; Stanton et al. 1994; Trevorrow & Tanaka 1997). At present there is no universally applicable scattering model. Current literature has focused almost entirely on euphausiids and copepods. The general modeling approach approximates the zooplankter as

an idealized shape of fluid-like material having a small contrast in density and sound speed relative to seawater. Usual modeling approximations are spherical or cylindrical, with the characteristic dimension usually taken as the equivalent spherical radius, *esr*. Purely empirical approaches are also employed, generally fitting a curve of the form $TS = A + B \cdot \log[\text{frequency}]$, where *TS* is target strength (=10·log[back-scatter cross-section] and A, B are constants. In general the acoustic scattering can be divided into two regimes: the *Rayleigh* regime at relatively low frequencies where the scattering cross-section increases as approximately the fourth-power of the acoustic wave-number (k), and the higher-frequency *geometric* regime where there is a weaker (or no) frequency dependence. The transition region between these regimes lies near $k \cdot esr \approx 1$. In the Rayleigh regime the particular choice of scattering model is less important, so a spherical approximation is usual. Through the transition region into the geometric regime, the choice of scattering model is becomes more important as the effects of zooplankter elongation, curvature, and orientation become more important. For example, Trevorrow & Tanaka (1997) found that a cylindrical model for 9 mm long amphipods better fit the measured scattering strengths in the 50 to 200 kHz transition region.

Figures 16 and 17 show comparisons of modeling and measurements for the two dominant classes of zooplankton. The various semi-analytic scattering models are taken from Stanton (1989), with the exception of empirical models for euphausiids from Kristensen & Dahlen (1986) and for copepods from Greenlaw (1977). For the euphausiid case the empirical model provides the best fit, particularly in following the resonant peak near 80 kHz, whereas for the copepod case the fluid cylinder model appears to be the best match to the data. In the 100 to 500 kHz region relevant in this study, both classes of zooplankton show backscatter in the Rayleigh-geometric transition region, with a frequency dependence that is different for euphausiids and copepods. In the 100 to 500 kHz band copepods show an increasing target strength with frequency, whereas euphausiids have a roughly flat response. A further complicating issue for large, elongated zooplankters is the effect of orientation angle at horizontal incidence. At side incidence zooplankters will have a larger target strength than at head or tail incidence. Measurements or modeling of this effect has not been reported, as most investigators still use vertical echo-sounders. However, for the case of a horizontally incident sonar it is reasonable to assume a uniform distribution of angles and thus use an azimuthally averaged target strength. Furthermore, appropriate modeling of backscatter from other zooplankton types (e.g. Siphonophores, Medusae) has not been reported in the literature(to the best of the author's knowledge), but as mentioned earlier their scattering contribution can be ignored because of their relatively low abundance.

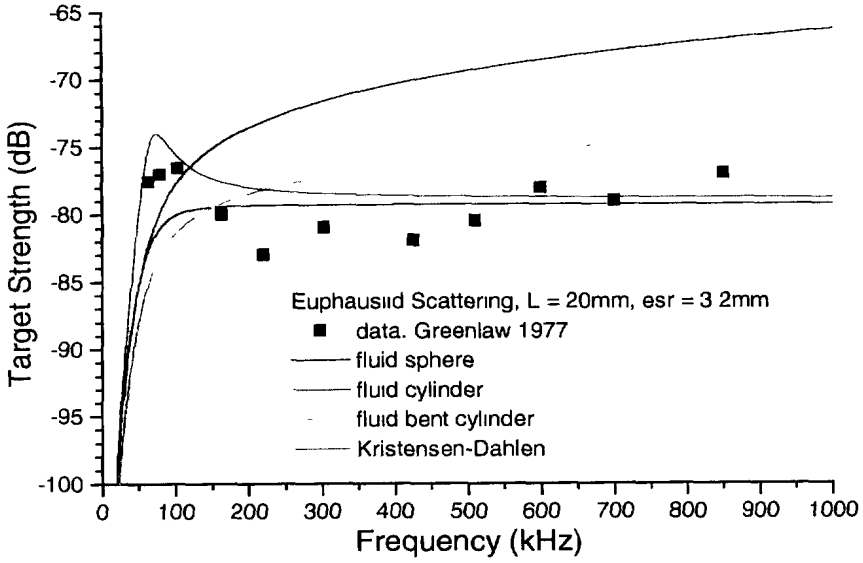

Figure 16: Comparison of various backscattering vs. frequency models with data for 20 mm long Euphausiids at dorsal/side incidence.

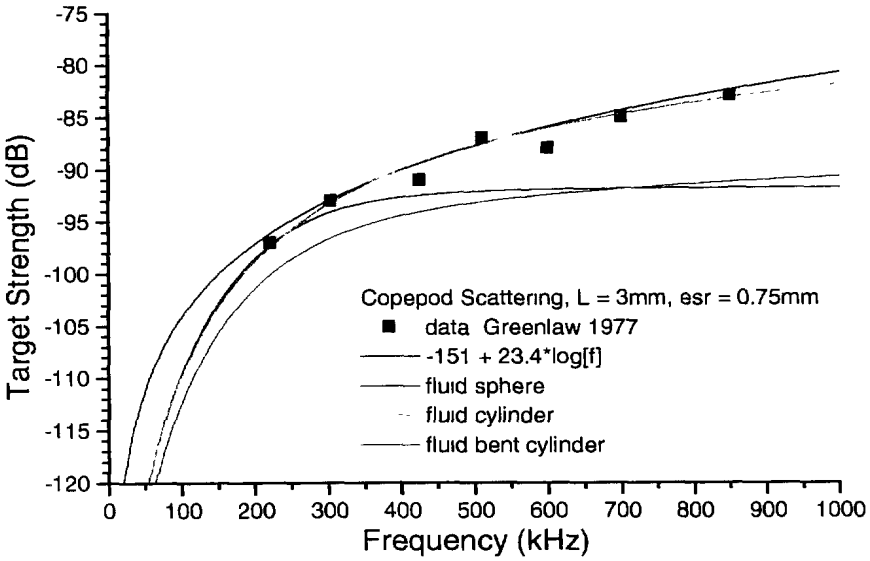

Figure 17: Comparison of various backscattering vs. frequency models with data for 3 mm long Copepods at dorsal/side incidence.

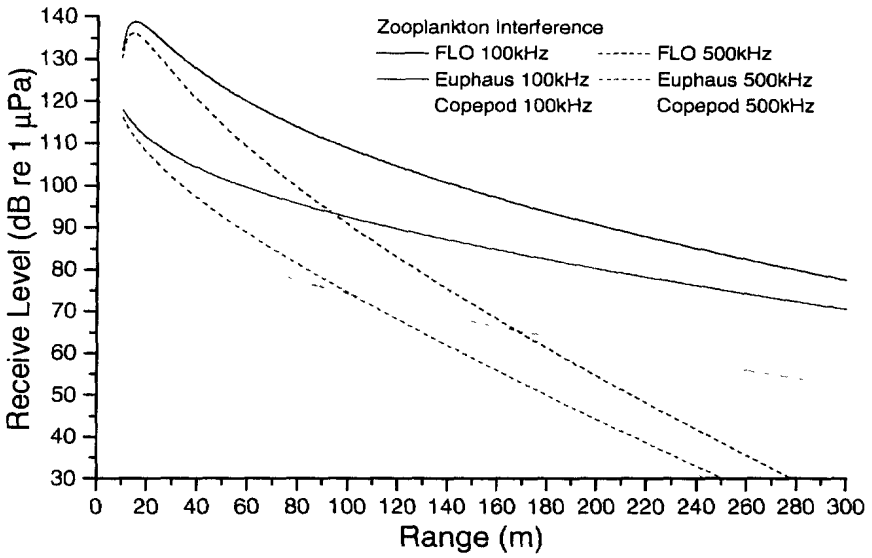

Figure 18: Comparison between RL for –15 dB FLO and euphausiid and copepod reverberation levels at 100 and 500 kHz. Assumes 1° horizontal by 20° vertical HF sonar at 3 m depth, with 4 mm length copepods at 5000 per m^3 and 20 mm euphausiids at 500 per m^3.

Finally, we can assess the potential interference due to copepods and euphausiids by assuming nominal size and abundance values, as shown in Figure 18. In this modeling the zooplankton layers are assumed to cause no acoustic extinction. At 100 kHz the euphausiid scattering starts out some 30 dB below the FLO receive level, but with increasing range the insonified volume of the sonar increases, causing the signal excess to decrease to roughly 6 dB by 300 m. At 100 kHz the copepod scattering level is roughly 20 dB less than for euphausiids and can be ignored. However, the copepod target strength increases with frequency such that by 500 kHz the copepod and euphausiid volume scattering strengths are comparable. At 500 kHz both zooplankton types have receive levels that approach the FLO echo to within 6 dB by 300 m range. Thus, under conditions of relatively high densities there is potential for zooplankton reverberation to interfere with OAS operations.

6. Summary Discussions:

With forward-looking HF sonar operations near the sea-surface, it is generally desirable to increase the operating range and to probe close to boundaries where targets or obstacles are often found. However, the near-surface environment creates several significant limitations to the use of such systems in low-grazing angle geometries, and these environmental influences must be included in design calculations. It can also be concluded from this work that it is imperative to monitor the oceanographic and meteorological conditions during OAS operations.

In particular, near-surface layers of microscopic air bubbles generated by white-capping processes have the potential to seriously inhibit OAS performance. Breaking-wave induced bubbles typically begin to appear above roughly 6 - 10 knots wind speed, and have a broad size distribution at radii from 10 to 400 μm. These micro-bubbles exhibit a strong volumetric backscatter, with maximum volume back-scattering strengths near –10 to 0 dB (re 1 m^{-1}). Furthermore, bubble layers can induce extinction losses of order 1 to 10 $dB \cdot m^{-1}$ depending on frequency. For typical AUV or RMV operating conditions (winds up to 20 knots), this bubble layer reverberation has the potential to obscure echoes from even large surface targets, and the bubble layer extinction strongly attenuates the signal from surface targets. The overall bubble effects are strongest in the 20 to 150 kHz frequency band, with expected FLO detection limited to less than 40 m in this band. However, positive signal to reverberation ratios up to 300 m range were predicted for higher frequency (300 to 400 kHz) systems, ultimately limited by dynamic range and other systemic noise performance issues. Bubbly ship wakes exhibit similar acoustic scattering and extinction properties.

Other potential sources of reverberative interference were investigated. Dense schools of fish (e.g. herring) have been found to exhibit echo strengths comparable to targets of interest, with spatial dimensions up to 20 to 30 m horizontally by 10 to 20 m vertically. Thus these schools would be readily detectable except under strong bubble conditions, and could be mis-interpreted as real targets or obstacles. Furthermore, in some locations and particularly at higher frequencies, reverberation from dense zooplankton (e.g. euphausiid and/or copepod) layers has the potential to interfere with, but not totally obscure, near-surface target detection. Finally, clutter due to backscatter from surface wave roughness at wind speeds up to 10 knots was found to not pose any significant limits on HF sonar performance.

Another important effect is acoustic refraction, which focuses acoustic energy upwards or downwards depending on the sound speed gradient. Strong sound speed gradients are common in coastal regions, especially near river-mouths, estuaries, fjords, or enclosed basins such as harbours. For OAS operations the most serious problems arise under downward-refracting conditions with the creation of near-surface acoustic shadow zones. In the example from the southern Strait of Georgia discussed herein, detection of sea-surface targets would not be possible for any HF OAS system beyond roughly 70 m range. Downward-refracting conditions would also arise in the case of bubble layer induced sound speed anomalies at frequencies above 100 kHz. Clearly, it now becomes an operational necessity to measure the sound speed vs. depth profiles and to model their influence on OAS performance.

In addition to boundary clutter and refraction, another confounding feature of near surface environments are multiple echoes from surface-reflected multi-paths. It is well known that *specular* acoustic reflections from the water surface will be nearly perfect at all angles, due to

the sharp contrast in sound speed and density between the two media. Only surface roughness due to wind-waves and extinction within a bubble layer will significantly effect the surface reflected echo intensity. At the small grazing angles under consideration here these direct and multi-path arrivals will typically overlap (i.e. the time delay between the two arrivals will be less than the pulse length), leading to interferences that will, in general, positively bias the estimated target strengths and increase the reverberation levels. In some situations this has a positive benefit in enhancing the SNR of these sub-surface targets, but will confound processing and detection algorithms sensitive to phase variations within a target echo (e.g. beam-forming or synthetic aperture techniques).

7. References:

Applied Physics Laboratory, University of Washington, 1994. APL-UW High-frequency ocean environmental acoustic models handbook. APL-UW TR 9407, Seattle, WA.

Crawford, G., and Farmer, D., 1987. On the spatial distribution of ocean bubbles. *J. Geophys. Res.* **92**(C8): 8231-8243.

Dahl, P., Nützel, B., Schmidt, A., Herwig, H., and Terray, E., 1997. Simultaneous acoustic and microwave backscattering from the sea surface. *J. Acoust. Soc. Am.* **101**(5): 2583-2595.

Farmer, D., Vagle, S., and Booth, A. D., 1998. A free-flooding acoustical resonator for measurement of bubble size distributions. *J. Atmos. Oceanic Tech.* **15**: 1132-1146.

Francois, R., and Garrison, G., 1982. Sound absorption based on ocean measurements, part II: Boric acid contribution and equation for total absorption. *J. Acoust. Soc. Am.* **72**: 1879-1890.

Fortuin, L, 1970. Survey of literature on reflection and scattering of sound waves at the sea surface. *J. Acoust. Soc. Am.* **47**(5): 1209-1228.

Garrett, C., Li, M., and Farmer, D., 2000. The connection between bubble size spectra and energy dissipation rates in the upper ocean. *J. Phys. Oceanogr.* **30**: 2163-2171.

Garrison, G., Murphy, S., and Potter, D., 1960. Measurements of the backscattering of underwater sound from the sea surface. *J. Acoust. Soc. Am.* **32**(1): 104-111.

Greene, C., P. Wiebe, and J. Burczynski, 1989. Analyzing zooplankton size distributions using high-frequency sound, *Limnol. Oceanogr.* **34**(1): 129-139.

Greenlaw, C., 1977. Backscattering spectra of preserved zooplankton, *J. Acoust. Soc. Am.* **62**(1): 44-52.

Hall, M., 1989. A comprehensive model of wind-generated bubbles in the ocean and predictions of the effects on sound propagation at frequencies up to 40 kHz. *J. Acoust. Soc. Am.* **86**(3): 1103-1117.

Holliday, D. V., and R. Pieper, 1980. Volume scattering strengths and zooplankton distributions at acoustic frequencies between 0.5 and 3 MHz, *J. Acoust. Soc. Am.* **67**(1): 135-146.

Johnson, R., 1977. Sound scattering from a fluid sphere revisited, *J. Acoust. Soc. Am.*, **61**, 375-377.

Johnson, B., and Cooke, R., 1979. Bubble populations and spectra in coastal waters: a photographic approach. *J. Geophys. Res.* **84**(C7): 3761-3766.

Kristensen, A., and J. Dahlen, 1986. Acoustic estimation of size distributions and abundance of zooplankton, *J. Acoust. Soc. Am.* **80**(2): 601-611.

Lamarre, E., and Melville, W., 1994. Sound speed measurements near the ocean surface. *J. Acoust. Soc. Am.* **96**(6): 3605-3616.

Macaulay, M., 1994. A generalized target strength model for euphausiids, with applications to other zooplankton, *J. Acoust. Soc. Am.* **95**(5): 2452-2466.

McDaniel, S., and Gorman, A., 1982. Acoustic and radar sea surface backscatter. *J. Geophys. Res.* **87**(C6): 4127-4136.

McDaniel, S., 1993. Sea surface reverberation: a review. *J. Acoust. Soc. Am.* **94**(4): 1905-1922.

Medwin, H., and Breitz, N., 1989. Ambient and transient bubble spectral densities in quiescent seas and under spilling breakers. *J. Geophys. Res.* **94**(C9): 12751-12759.

Medwin, H., and Clay, C., 1998. *Fundamentals of Acoustical Oceanography* (Academic Press, San Diego).

Novarini, J., and Bruno, D., 1982. Effects of the sub-surface bubble layer on sound propagation. *J. Acoust. Soc. Am.* **72**(2): 510-514.

Nützel, B., Herwig, H., Koenigs, P., and Monti, J., 1994. Acoustic backscatter measurements in the North Sea: 3 – 18 kHz. *J. Acoust. Soc. Am.* **95**(5): 2488-2494.

Reeves, J., Igarashi, Y., Beck, L., and Stern, R., 1969. Azimuthal dependence of sound backscattered from the sea surface. *J. Acoust. Soc. Am.* **46**(5): 1284-1288.

Stanton, T. K., 1989. Simple approximate formulas for backscattering of sound by spherical and elongated objects. *J. Acoust. Soc. Am.* **86**(4): 1499-1510.

Stanton, T., Wiebe, P., Chu, D., Benfield, M., Scanlon, L., Martin, L., and Eastwood, R., 1994. On acoustic estimates of zooplankton biomass. *ICES J. Mar. Sci.* **51**: 505-512.

Thorpe, S., 1982. On the clouds of bubbles formed by breaking wind-waves in deep water and their role in air-sea gas transfer. *Phil. Trans. Roy. Soc. London* **A304**: 155-210.

Trevorrow, M., Vagle, S., and Farmer, D., 1994. Acoustic measurements of micro bubbles within ship wakes. *J. Acoust. Soc. Am.* **95**(4): 1922-1930.

Trevorrow, M., 1996. Multi-frequency acoustic measurements of near-surface air bubbles in Lake Biwa. *Japanese J. Limnology* **57** (4): 411-423.

Trevorrow, M., and Y. Tanaka, 1997. Acoustic and in situ measurements of freshwater amphipods (*Jesogammarus annandalei*) in Lake Biwa, Japan, *Limnol. Oceanogr.* **42**(1): 121-132.

Trevorrow, M., 1997. Detection of migrating salmon in the Fraser River using 100-kHz sidescan sonar. *Can. J. Fish. Aquat. Sci.* **54**: 1619-1629.

Trevorrow, M., and Pedersen, B., 1999. Continuous monitoring of fish in a shallow channel using fixed horizontal sonar. *J. Acoust. Soc. Am.* **105**(6): 3126-3135.

Vagle, S., and Farmer, D., 1992. The measurement of bubble-size distributions by acoustical backscatter. *J. Atmos. Oceanic Technol.* **9**(5): 630-644.

Vagle, S., and Farmer, D., 1998. A comparison of four methods for bubble size and void fraction measurements. *IEEE J. Oceanic Eng.* **23**(3): 211-222.

Walsh, A., and Mulhearn, P., 1987. Photographic measurements of bubble populations from breaking wind waves at sea. *J. Geophys. Res.* **92**(C13): 14553-14565.

Wiebe, P. Greene, C., Stanton, T., and Burczynski, J., 1990. Sound scattering by live zooplankton and micronekton: empirical studies with a dual-beam acoustical system. *J. Acoust. Soc. Am.* **88**(5), 2346-2360.

Wu, J., 1988. Bubbles in the near-surface ocean: a general description. *J. Geophys. Res.* **93**(C1): 587-590.

UNCLASSIFIED
SECURITY CLASSIFICATION OF FORM
(highest classification of Title, Abstract, Keywords)

DOCUMENT CONTROL DATA

(Security classification of title, body of abstract and indexing annotation must be entered when the overall document is classified)

1 ORIGINATOR (the name and address of the organization preparing the document.. Organizations for whom the document was prepared, e.g. Establishment sponsoring a contractor's report, or tasking agency, are entered in section 8)

Defence Research Establishment Atlantic
PO Box 1012
Dartmouth, Nova Scotia, Canada B2Y 3Z7

2 SECURITY CLASSIFICATION (overall security classification of the document including special warning terms if applicable)

UNCLASSIFIED

3 TITLE (the complete document title as indicated on the title page. Its classification should be indicated by the appropriate abbreviation (S,C,R or U) in parentheses after the title)

Near-surface environmental limitations to high-frequency sonar performance: a review (U)

4 AUTHORS (Last name, first name, middle initial If military, show rank, e.g. Doe, Maj John E.)

Trevorrow, Mark V.

5 DATE OF PUBLICATION (month and year of publication of document)	6a NO .OF PAGES (total containing information Include Annexes, Appendices, etc)	6b NO OF REFS (total cited in document)
January 2001	36	37

7 DESCRIPTIVE NOTES (the category of the document, e g. technical report, technical note or memorandum. If appropriate, enter the type of report, e.g interim, progress, summary, annual or final Give the inclusive dates when a specific reporting period is covered)

TECHNICAL MEMORANDUM

8 SPONSORING ACTIVITY (the name of the department project office or laboratory sponsoring the research and development Include address)

Defence Research Establishment Atlantic

9a PROJECT OR GRANT NO (if appropriate, the applicable research and development project or grant number under which the document was written Please specify whether project or grant)	9b CONTRACT NO. (if appropriate, the applicable number under which the document was written)
1DA	

10a ORIGINATOR'S DOCUMENT NUMBER (the official document number by which the document is identified by the originating activity This number must be unique to this document)	10b OTHER DOCUMENT NOs (Any other numbers which may be assigned this document either by the originator or by the sponsor)
DREA TM 2001-002	

11 DOCUMENT AVAILABILITY (any limitations on further dissemination of the document, other than those imposed by security classification)

(✔) Unlimited distribution
( ) Defence departments and defence contractors; further distribution only as approved
( ) Defence departments and Canadian defence contractors; further distribution only as approved
( ) Government departments and agencies; further distribution only as approved
( ) Defence departments; further distribution only as approved
( ) Other (please specify):

12 DOCUMENT ANNOUNCEMENT (any limitation to the bibliographic announcement of this document. This will normally correspond to the Document Availability (11) However, where further distribution (beyond the audience specified in (11) is possible, a wider announcement audience may be selected)

UNCLASSIFIED
SECURITY CLASSIFICATION OF FORM
(highest classification of Title, Abstract, Keywords)

13 ABSTRACT *(a brief and factual summary of the document It may also appear elsewhere in the body of the document itself It is* highly desirable that the abstract of classified documents be unclassified Each paragraph of the abstract shall begin with an indication of the security classification of the information in the paragraph (unless the document itself is unclassified) represented as (S), (C), (R), or (U) It is not necessary to include here abstracts in both official languages unless the text is bilingual)

This work reviews relevant environmental constraints on the performance of high-frequency forward-looking obstacle or mine avoidance sonars. These high-resolution, narrow-beam systems typically operate at frequencies 100 - 500 kHz, focused on detection and classification of near-surface targets up to 500 m range. Relative signal-to-reverberation performance vs. range for a –15 dB surface target is modeled using a generic sonar model approach. Reverberation from and absorption by near-surface micro-bubble layers is shown to create very strong interference. Breaking-wave induced bubbles typically begin to appear above 6 - 10 knots wind speed, with typical bubble density spectra strongly decreasing from 10 to 400 μm radius. At high-frequencies these micro-bubble layers exhibit strong volumetric backscatter, with maximum volumetric back-scattering strengths near –10 dB (re 1 m^{-1}), and strong extinction losses of order 1 $dB \cdot m^{-1}$. Detectability of surface targets is limited to less than 20 m at 100 kHz, but the detection range increases with frequency to roughly 250 m at 400 kHz and above. Another significant performance limitation is acoustic refraction by near-surface sound speed gradients commonly found in coastal regions, especially near river-mouths and estuaries and during summer months. The most serious problems arise under downward-refracting conditions with the creation of near-surface acoustic shadow zones. Ray-tracing predictions under typical summertime coastal conditions show surface shadow regions (i.e. zero detectability) beyond 80 m range. Reverberation from dense zooplankton layers and schooling fish is shown to create minor levels of interference. Reverberation from surface wave roughness scattering in the absence of bubbles is shown to have negligible impact. (U)

14. KEYWORDS, DESCRIPTORS or IDENTIFIERS *(technically meaningful terms or short phrases that characterize a* document and could be helpful in cataloguing the document They should be selected so that no security classification is required Identifiers, such as equipment model designation, trade name, military project code name, geographic location may also be included If possible keywords should be selected from a published thesaurus. e g Thesaurus of Engineering and Scientific Terms (TEST) and that thesaurus-identified If it not possible to select indexing terms which are Unclassified, the classification of each should be indicated as with the title)

high-frequency sonar, micro-bubbles, reverberation, refraction, zooplankton

Defence R&D Canada
is the national authority for providing
Science and Technology (S&T) leadership
in the advancement and maintenance
of Canada's defence capabilities.

R et D pour la défense Canada
est responsable, au niveau national, pour
les sciences et la technologie (S et T)
au service de l'avancement et du maintien des
capacités de défense du Canada.

DEFENCE R&D DÉFENSE

www.drdc-rddc.dnd.ca